nature research

https://doi.org/10.1038/s41563-020-0755-z

## Supplementary information

# The dose threshold for nanoparticle tumour delivery

In the format provided by the authors and unedited

# The dose threshold for nanoparticle tumour delivery

**Authors:** Ben Ouyang[1,2,3], Wilson Poon[# 2,3], Yi-Nan Zhang[# 2,3], Zachary P. Lin[2,3], Benjamin R. Kingston[2,3], Anthony J. Tavares[2,3,4], Yuwei Zhang[3,5], Juan Chen[6], Michael S. Valic[6], Abdullah M. Syed[2,3,7], Presley MacMillan[3,5], Julien Couture-Senécal[2,3,8], Gang Zheng[2,6,9], Warren C.W. Chan[* 2,3,5,10,11]

**Affiliations:**

[1] MD/PhD Program, University of Toronto, Toronto, Ontario, Canada

[2] Institute Biomedical Engineering, University of Toronto, Toronto, Ontario, Canada.

[3] Terrence Donnelly Centre for Cellular and Biomolecular Research, University of Toronto, Toronto, Ontario, Canada.

[4] School of Life Sciences, Faculty of Humanities and Social Sciences, Sheridan College, Brampton, Ontario, Canada.

[5] Department of Chemistry, University of Toronto, Toronto, Ontario, Canada.

[6] Princess Margaret Cancer Centre, University Health Network, Toronto, Ontario, Canada.

[7] J. David Gladstone Institutes, San Francisco, CA, USA.

[8] Division of Engineering Science, University of Toronto, Toronto, Ontario, Canada.

[9] Department of Medical Biophysics, University of Toronto, Toronto, Ontario, Canada.

[10] Department of Chemical Engineering, University of Toronto, Toronto, Ontario, Canada.

[11] Department of Material Science and Engineering, University of Toronto, Toronto, Ontario, Canada.

[#] These authors contributed equally to this work.

*Correspondence to W.C.W.C. (email: warren.chan@utoronto.ca).

## Supplementary Figures

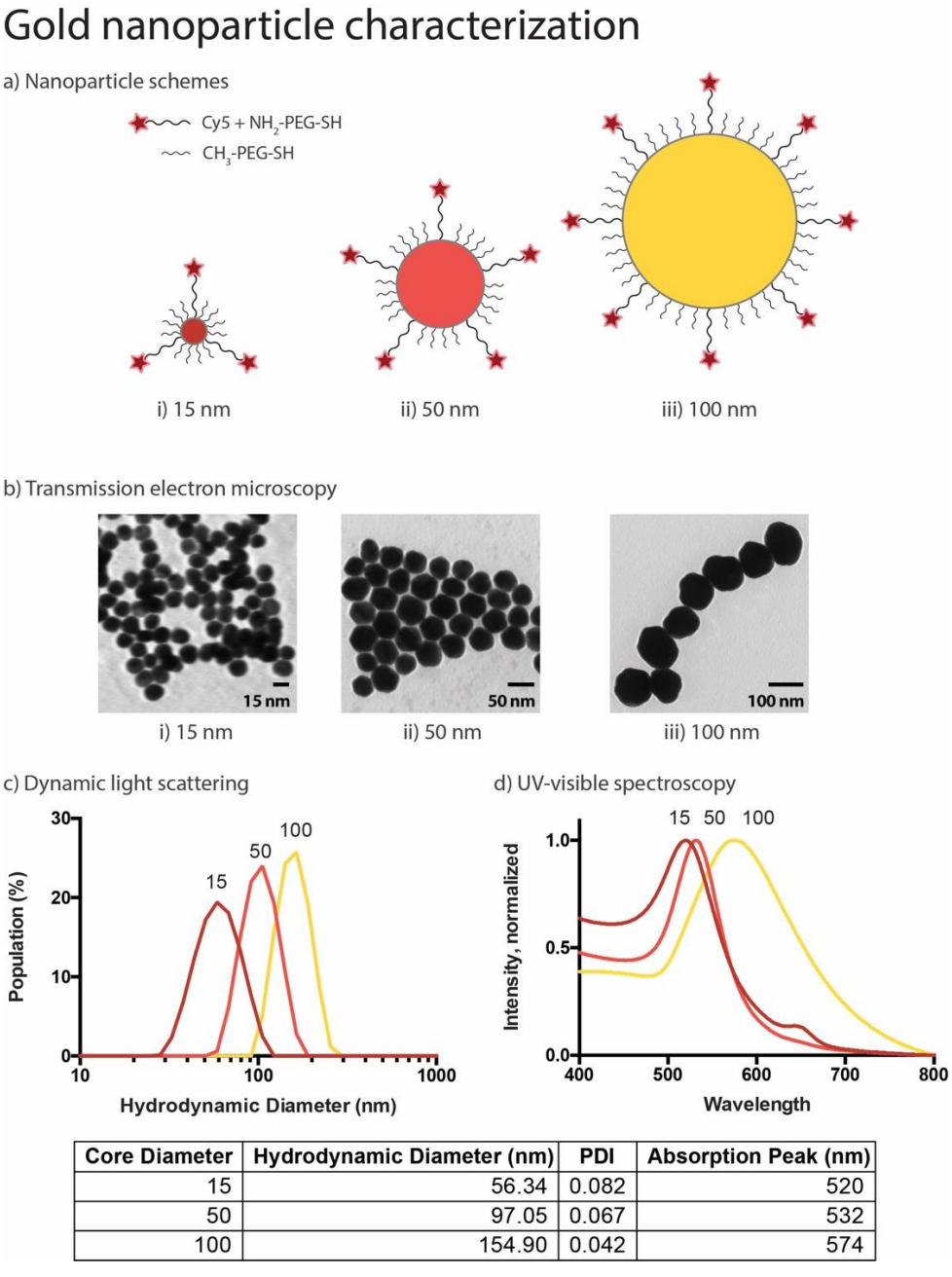


| Core Diameter | Hydrodynamic Diameter (nm) | PDI | Absorption Peak (nm) |
|---|---|---|---|
| 15 | 56.34 | 0.082 | 520 |
| 50 | 97.05 | 0.067 | 532 |
| 100 | 154.90 | 0.042 | 574 |

**Supplementary Figure 1 | Gold Nanoparticle Characterization**
**(a)** Schematics of gold nanoparticles ligand-stabilized using 5k mPEG and fluorescently labelled with 10k amine-terminated poly(ethylene glycol) conjugated to Cy5 in 3 sizes: **(i)** 15 nm, **(ii)** 50 nm, **(iii)** 100 nm. **(b)** Transmission electron microscopy images of **(i)** 15 nm, **(ii)** 50 nm, **(iii)** 100 nm gold nanoparticles. Scale bars as indicated in images. **(c)** Dynamic light scattering measurements of hydrodynamic diameters of gold nanoparticles. **(d)** UV-visible spectroscopy of gold nanoparticles. The absorption shoulder at 647 nm is the absorbance band of Cy5, which is visible over the gold absorbance mostly in 15 nm nanoparticles and some in 50 nm nanoparticles.

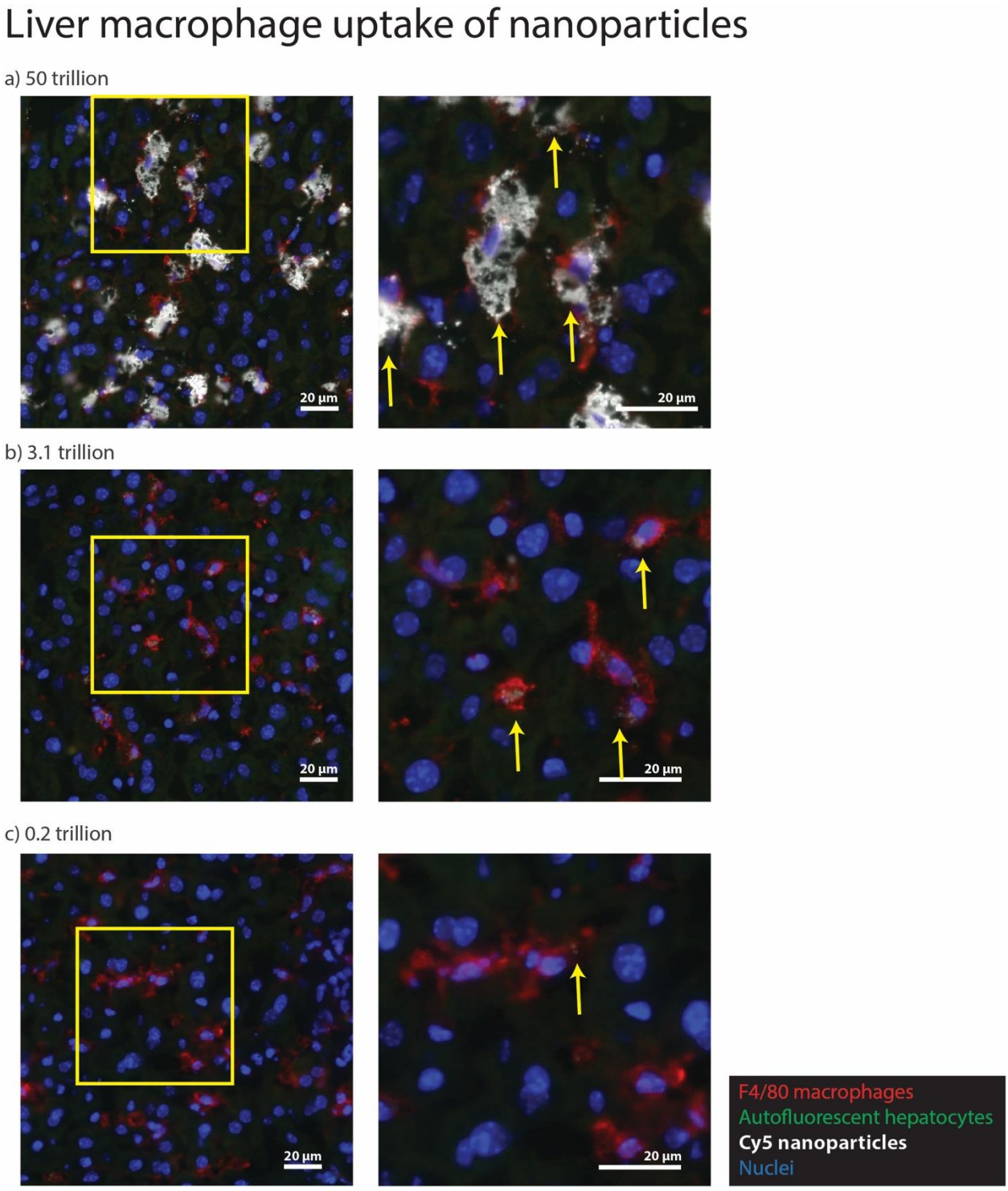


**Supplementary Figure 2 | Liver macrophage uptake quantification by histology**
Representative images used for quantification in Figure 1e. Macrophages were manually traced around F4/80$^{+}$ (red) regions in ImageJ, and this was used as a mask to quantify the nanoparticle (white) accumulation. Nanoparticles of 20 randomly-selected macrophages were quantified per slide. Average nanoparticle signal per cell was divided by the dose of nanoparticles injected to obtain graph in Figure 1e.

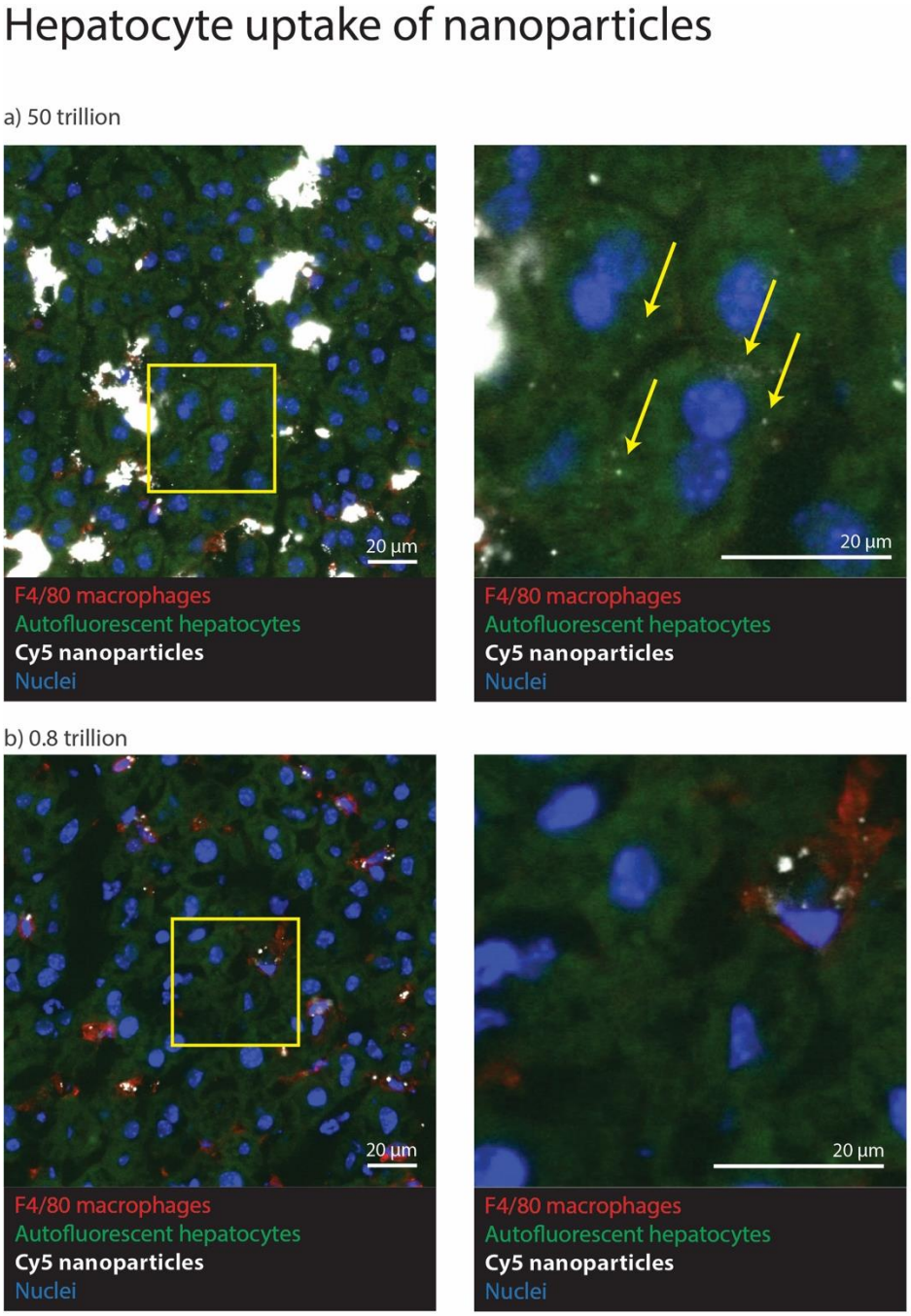


**Supplementary Figure 3 | Hepatocyte nanoparticle uptake beyond dose threshold**
Representative images used in quantification in Figure 1e (inset). **(a)** Hepatocytes (green) took up nanoparticles (white) at a bolus dose of 50 trillion (yellow arrows). **(b)** Nanoparticles in hepatocytes were undetectable at doses lower than 1 trillion.

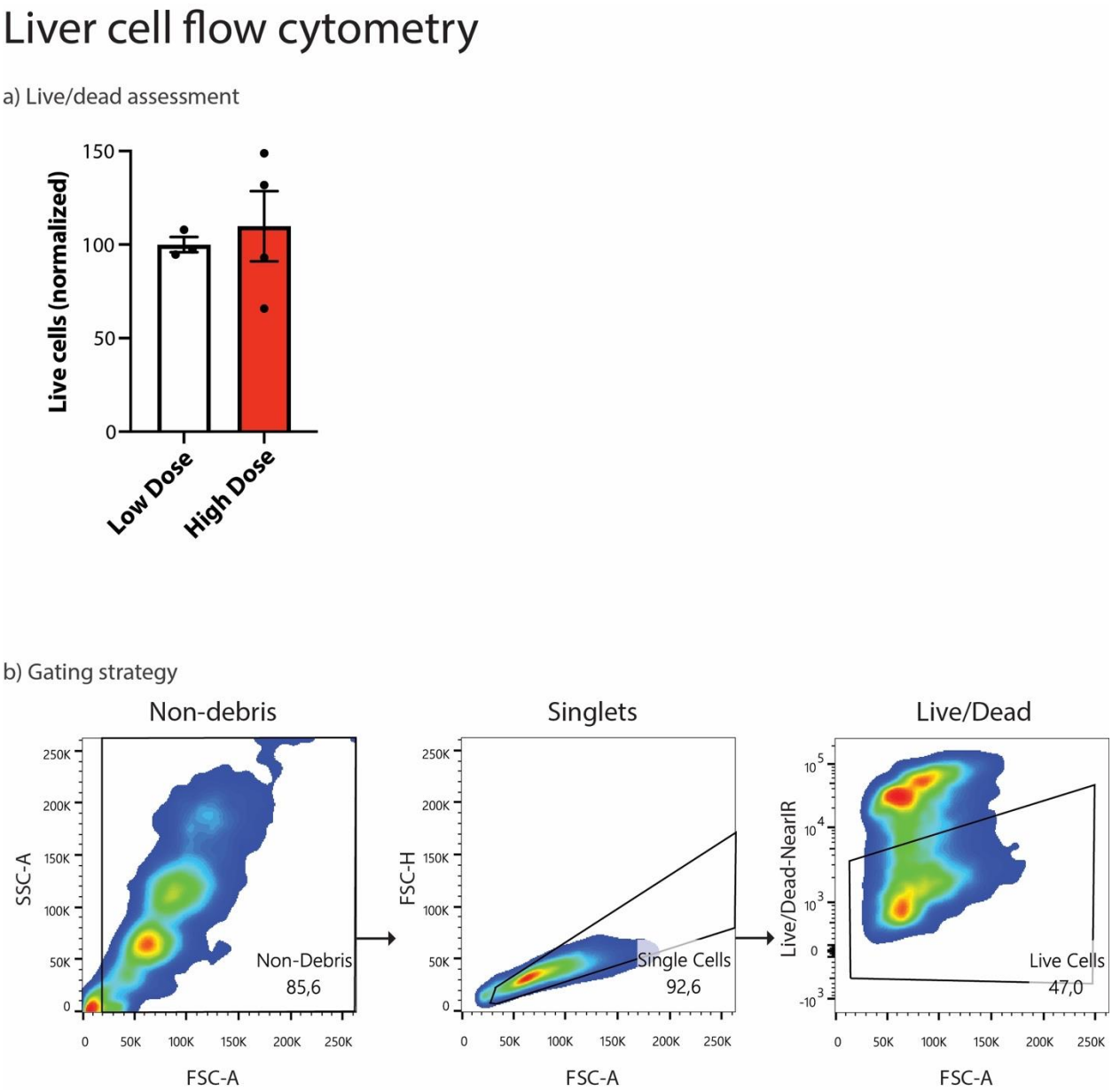


**Supplementary Figure 4 | Flow cytometry live/dead analysis of liver cells at different doses** **(a)** Quantification of live cells in the liver of mice administered with a low dose (0.2 trillion) or high dose (50 trillion) PEGylated gold nanoparticles, 24 hours after injection. Survival was normalized to the proportion of live cells in the low dose condition. High dose live cell proportion was not different than low dose live cell proportion. All data points and error bars represent the mean ± s.e.m. n = 3. Statistical significance was evaluated using a two-tailed unpaired t-test. (p = 0.6784). **(b)** Representative gating strategy used to identify proportion of live cells.

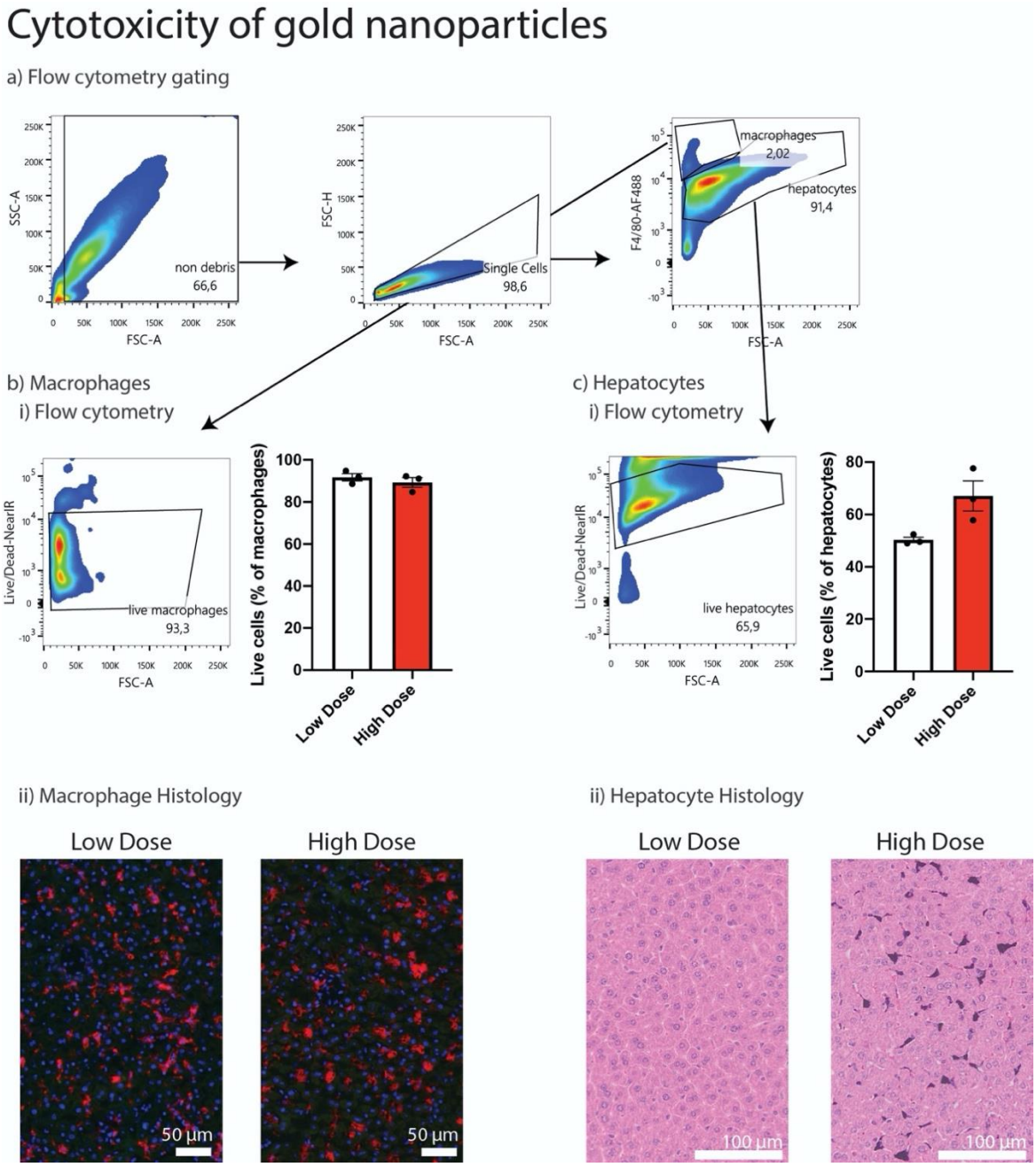


**Supplementary Figure 5 | Cytotoxicity of gold nanoparticles at low and high doses**
There was no observable effect of dose on the cytotoxicity of macrophages and hepatocytes in the range of doses studied. **(a)** Gating strategy used to identify macrophages and hepatocytes. **(b) (i)** A live/dead stain was used to identify live macrophages. n=3. **(ii)** A cryosection of liver dosed with low or high numbers of nanoparticles. Blue is DAPI, red is F4/80+ cells and nanoparticles, and green is autofluorescence (hepatocytes). **(c) (i)** A live/dead stain was used to identify live hepatocytes. n=3. **(ii)** A paraffin-fixed section of liver dosed with low or high numbers of nanoparticles. H&E stained. All data points and error bars represent the mean ± s.e.m. Statistical significance was evaluated using a two-tailed unpaired t-test. All micrographs are representatives of n=3 biological replicates across 1 independent experiment.

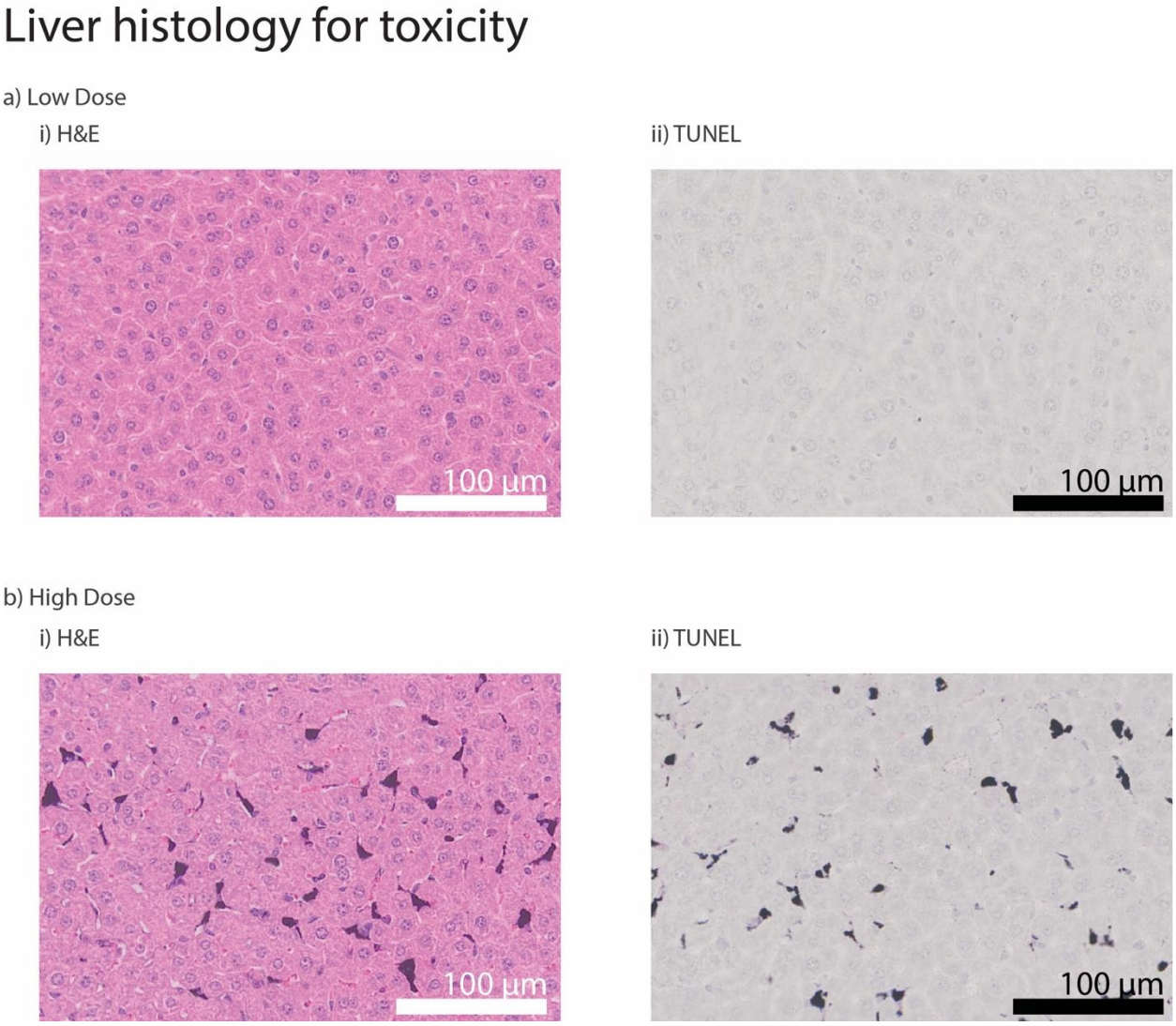


**Supplementary Figure 6 | Histology of liver at high and low doses of gold nanoparticles** **(a)** Representative image of a liver of a mouse administered with a low dose (0.2 trillion) of gold nanoparticles, stained with **(i)** H&E and **(ii)** TUNEL. **(b)** Representative image of a liver of a mouse administered with a high dose (50 trillion) of gold nanoparticles, stained with **(i)** H&E and **(ii)** TUNEL. The dark purple are gold nanoparticles that have accumulated in the sinusoidal cells. Note that no nuclei have stained positive for TUNEL. H&E micrographs representative of n=6 animals from 2 independent experiments. TUNEL micrographs representative of n=3 animals from 1 experiment.

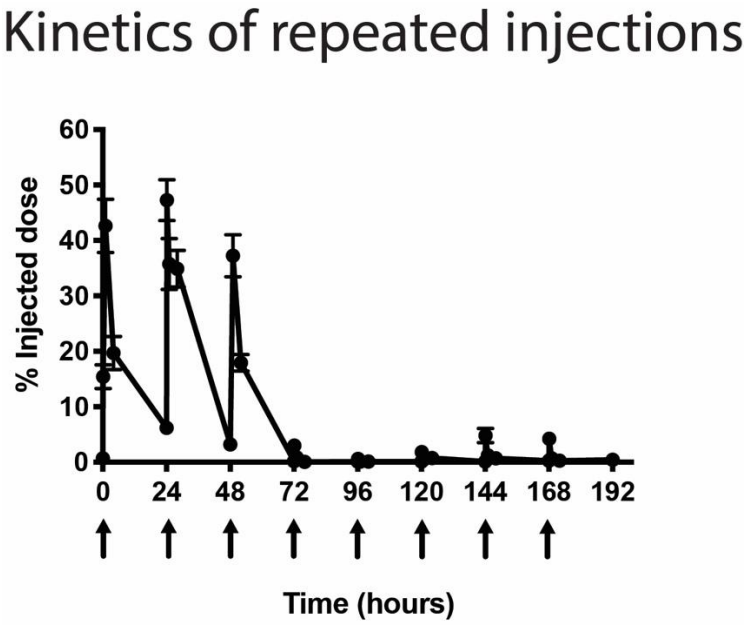


**Supplementary Figure 7 | Blood clearance of daily repeated low dose injections**
Gold nanoparticles were injected daily (arrows). Blood was collected at the following timepoints: just before injection, 10 minutes, 1 hour, 4 hours. On day 4, there was a sudden acceleration of blood clearance, in agreement with the accelerated blood clearance (ABC) phenomenon. All data points and error bars represent the mean ± s.e.m. (n = 3).

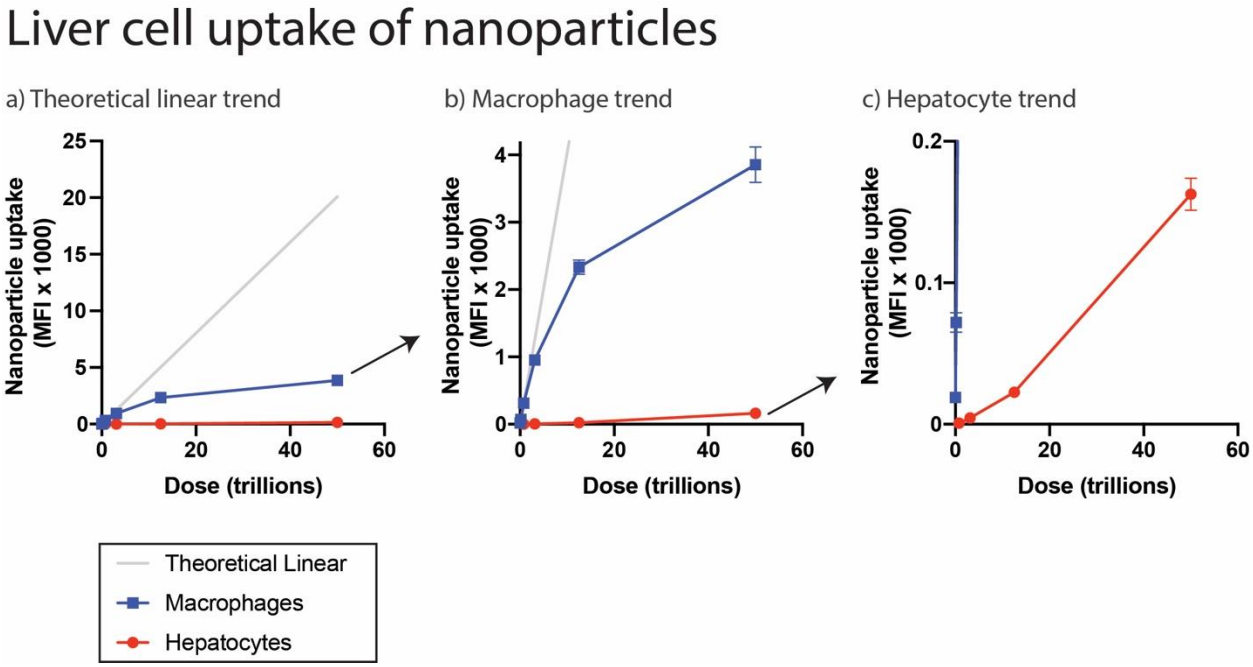


**Supplementary Figure 8 | Non-normalized uptake intensities of liver cells**
Additional graphs for Figure 1e without dose normalization. **(a)** Liver cell uptake (blue, red) compared against a linearly-increasing trend, by extrapolating from the linear intensity increase in liver macrophages in doses up to 0.80 trillion nanoparticles. **(b)** Zoom in of (a). Kupffer cell uptake was proportionally less with increasing dose, but not completely saturated. **(c)** Zoom in of (b). Hepatocyte uptake of nanoparticles increased with increasing dose. All data points and error bars represent mean ± s.e.m. n = 30 cells from 3 mice.

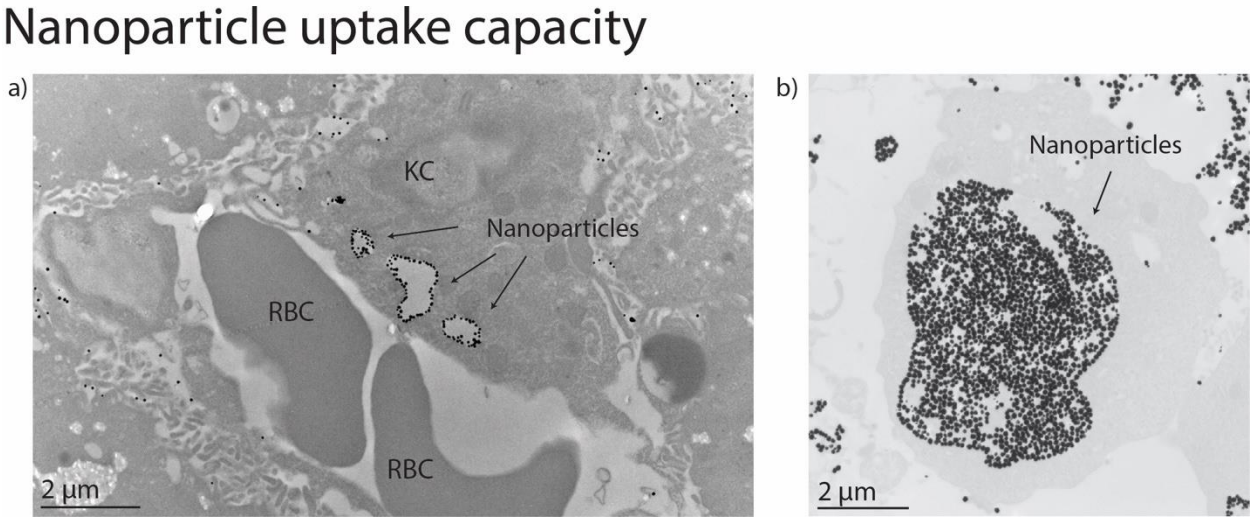


**Supplementary Figure 9 | Nanoparticle uptake capacity of macrophages**
**(a)** TEM imaging of a Kupffer cell in a liver sinusoid 30 minutes after nanoparticle injection. Note that the nanoparticles occupied a minor proportion of the Kupffer cell volume. KC: Kupffer Cell, RBC: Red Blood Cell. Representative image from n=3 animals from 2 independent experiments. **(b)** TEM imaging of a RAW264.7 macrophage incubated with nanoparticles for 24 hours, demonstrating the large nanoparticle uptake capacity of macrophages. Representative image from n=6 samples from 2 independent experiments.

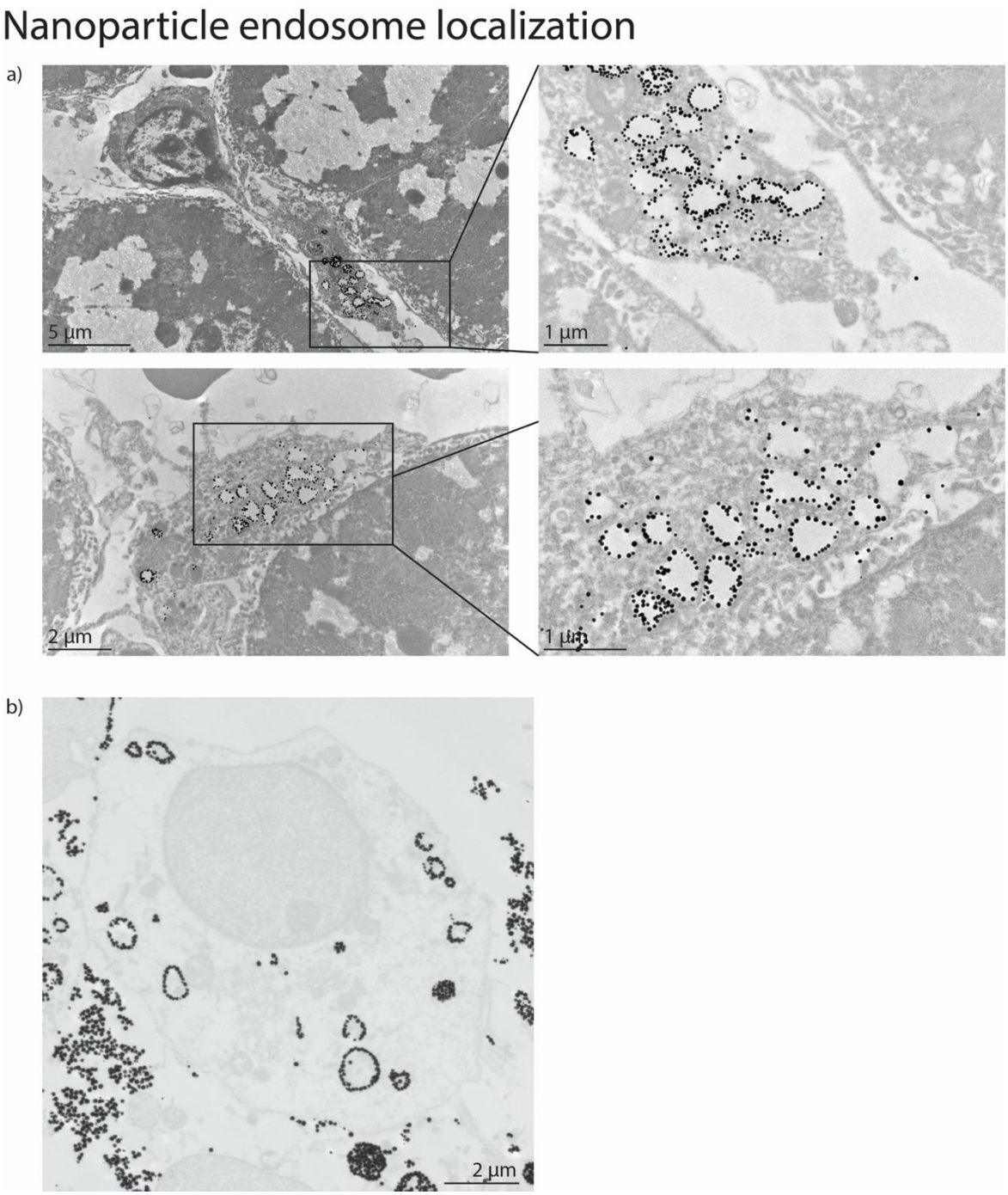


**Supplementary Figure 10 | Nanoparticles bind to membranes**
**(a)** Representative TEM images of Kupffer cells in liver sinusoids, 30 minutes after nanoparticle injection. Images on the right are higher magnifications. Nanoparticles are seen to line the perimeters of Kupffer cell endosomes, suggesting they were internalized after binding to the Kupffer cell membrane. Note the density of packing onto the endosomal membranes, with minimal available binding sites. Representative image from n=3 animals from 2 independent experiments. **(b)** Uptake into RAW264.7 macrophages *in vitro* shows similar pattern of endosome membrane binding. Representative image from n=6 samples from 2 independent experiments.

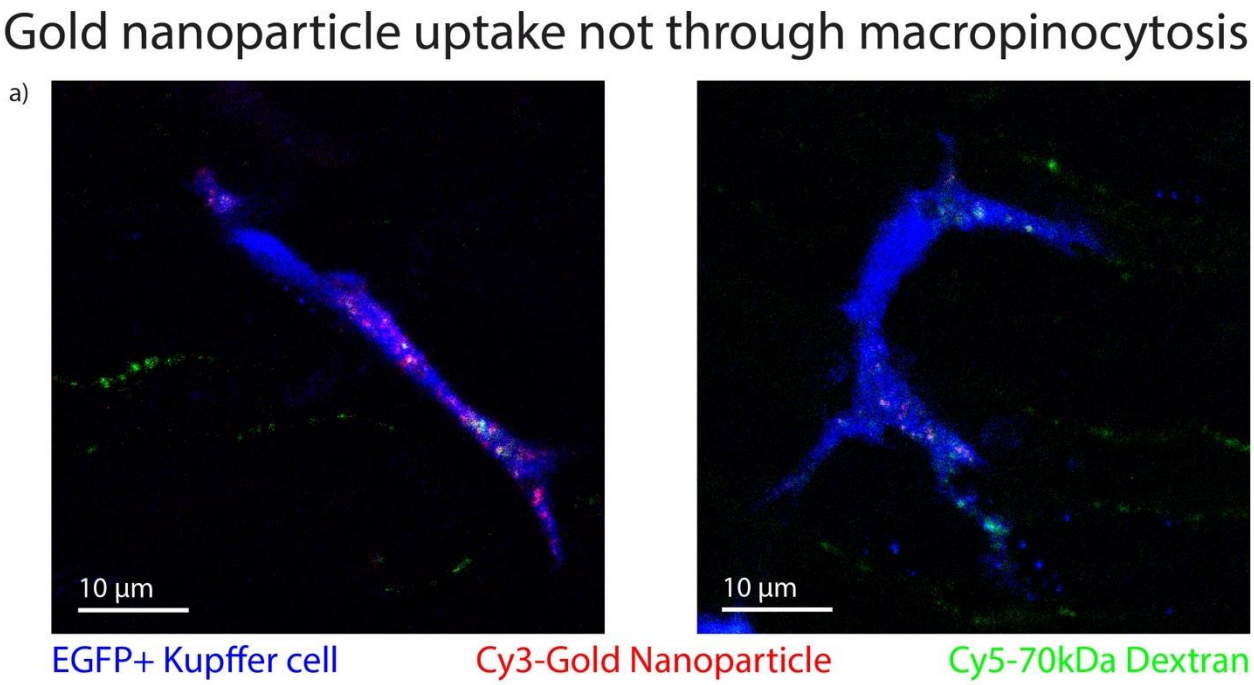


**Supplementary Figure 11 | Gold nanoparticle co-localization with 70 kDa dextran** **(a)** Representative images of live single-cell *in vivo* intravital microscopy images, 1 hour after co-injection of 0.2 trillion gold nanoparticles with 1 mg/mL dextran-70 kDa. Kupffer cells (blue) took up gold C3-labelled gold nanoparticles (red) and Cy5-labelled 70 kDa dextran (green) into different subcellular locations. **(b)** Quantification of co-localization of gold and dextran by Pearson's r and Mander's M coefficients. Low correlation suggested gold nanoparticles were taken up by a different pathway than macropinocytosis (dextran).

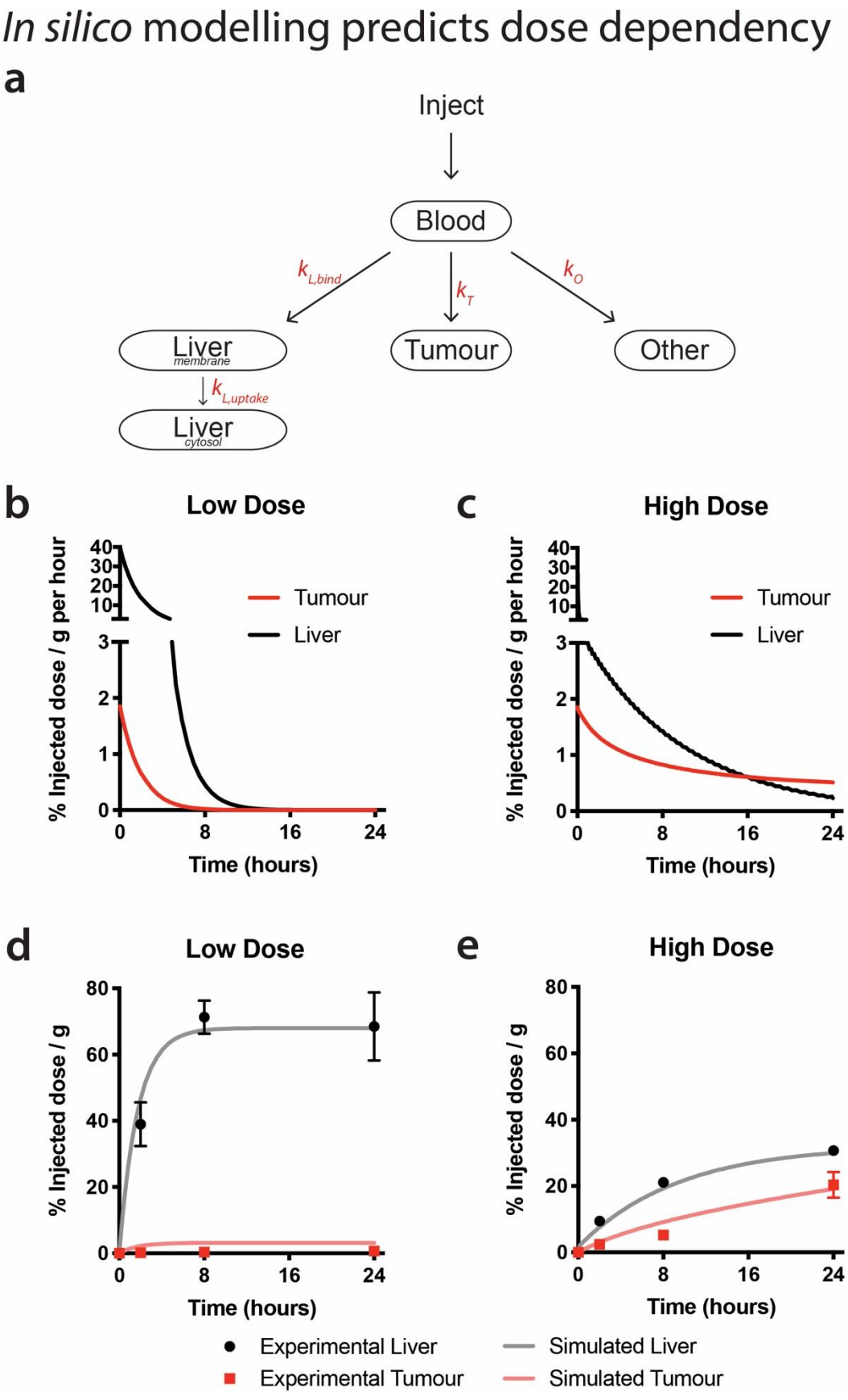
*In silico* modelling predicts dose dependency
a
Inject
Blood
$k_{L,bind}$
$k_T$
$k_O$
Liver membrane
Tumour
Other
$k_{L,uptake}$
Liver cytosol
b
Low Dose
% Injected dose / g per hour
Tumour
Liver
Time (hours)
c
High Dose
% Injected dose / g per hour
Tumour
Liver
Time (hours)
d
Low Dose
% Injected dose / g
Time (hours)
e
High Dose
% Injected dose / g
Time (hours)
Experimental Liver
Experimental Tumour
Simulated Liver
Simulated Tumour

1

**Supplementary Figure 12 | Compartment modelling predicts kinetic delivery to tumours** **(a)** Compartment model. Nanoparticles injected into the blood transfer into peripheral organs (liver, tumour, and others) with individual rate constants *k*. Nanoparticle transfer back into blood was assumed to be negligible. $k_{L,bind}$, transport rate constant from blood to liver Kupffer cell membranes, $k_{L,uptake}$, transport rate constant from Kupffer cell membranes to Kupffer cell endosomes, $k_T$, transport rate constant from blood to tumour, $k_O$, transport rate constant from blood to other organs. **(b,c)** Simulated accumulation rates in the liver (black) and tumour (red) when given a low dose of 0.2 trillion nanoparticles **(b)** and high dose of 50 trillion nanoparticles **(c)**. **(d,e)** Total accumulation in the liver (gray, black) and tumour (pink, red) when given a low dose **(d)** and high dose **(e)** of nanoparticles. Experimental data at 2 hours, 8 hours, and 24 hours post injection overlaid onto simulated data. n = 3 for each experimental point. All data points and error bars represent mean ± s.e.m.

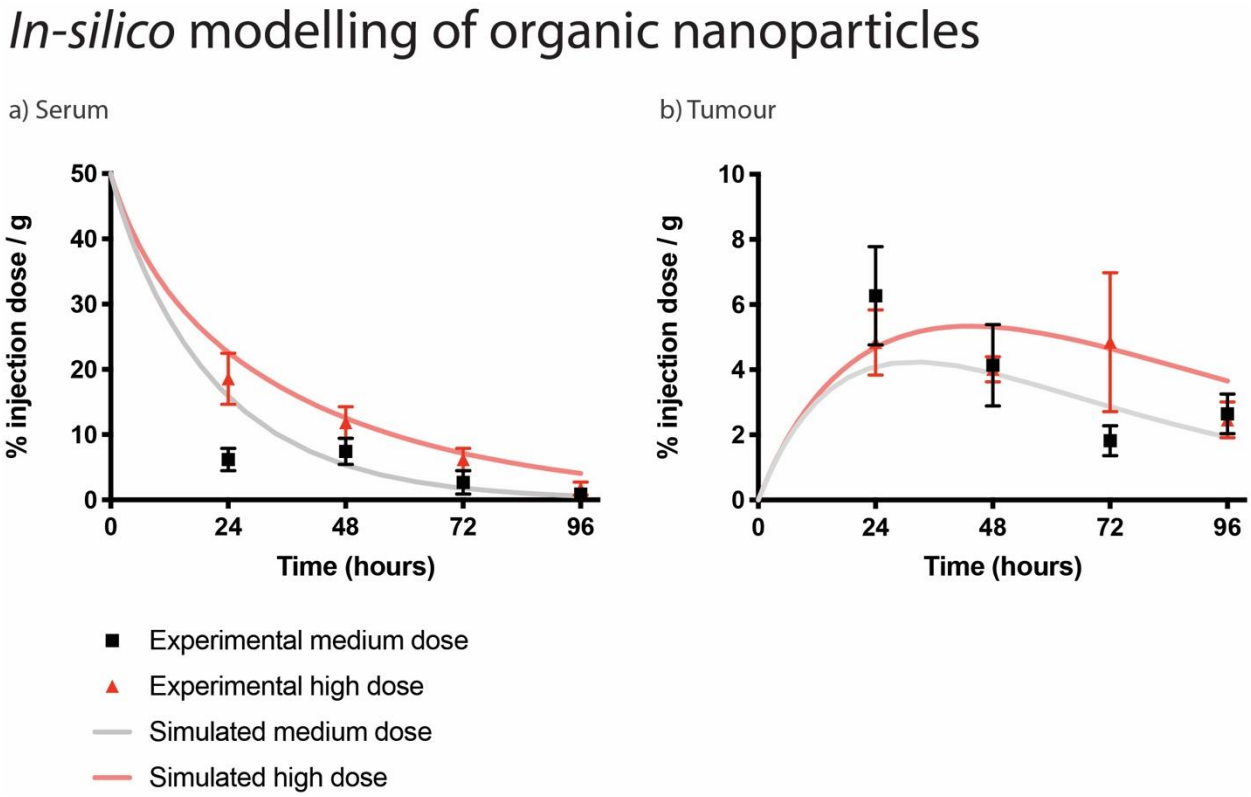


**Supplementary Figure 13 | In-silico model adapted for degradable organic nanoparticles** The *in-silico* model of Supplementary Figure 12 was adapted for organic nanoparticles by adding a degradation term (see methods). Since a different nanoparticle was used in this model, affinity constants $k_{liver}$, $k_{tumour}$, and $k_{others}$ were modified compared to gold nanoparticles. Caelyx was used as the experimental nanoparticle to compare to the modelling results, and its dose was increased by injecting Caelyx-like liposomes without doxorubicin (Supplementary Figure 16, see experiment in Figure 5). **(a)** Elimination of Caelyx from serum for nanoparticles administered at a medium dose (4.6 trillion) or high dose (50 trillion). **(b)** Accumulation of Caelyx into tumours for nanoparticles administered at a medium dose (4.6 trillion) or high dose (50 trillion). All data points and error bars represent mean ± s.e.m. from n = 3 mice (24, 72 hours), n = 6 mice (48, 96 hours).

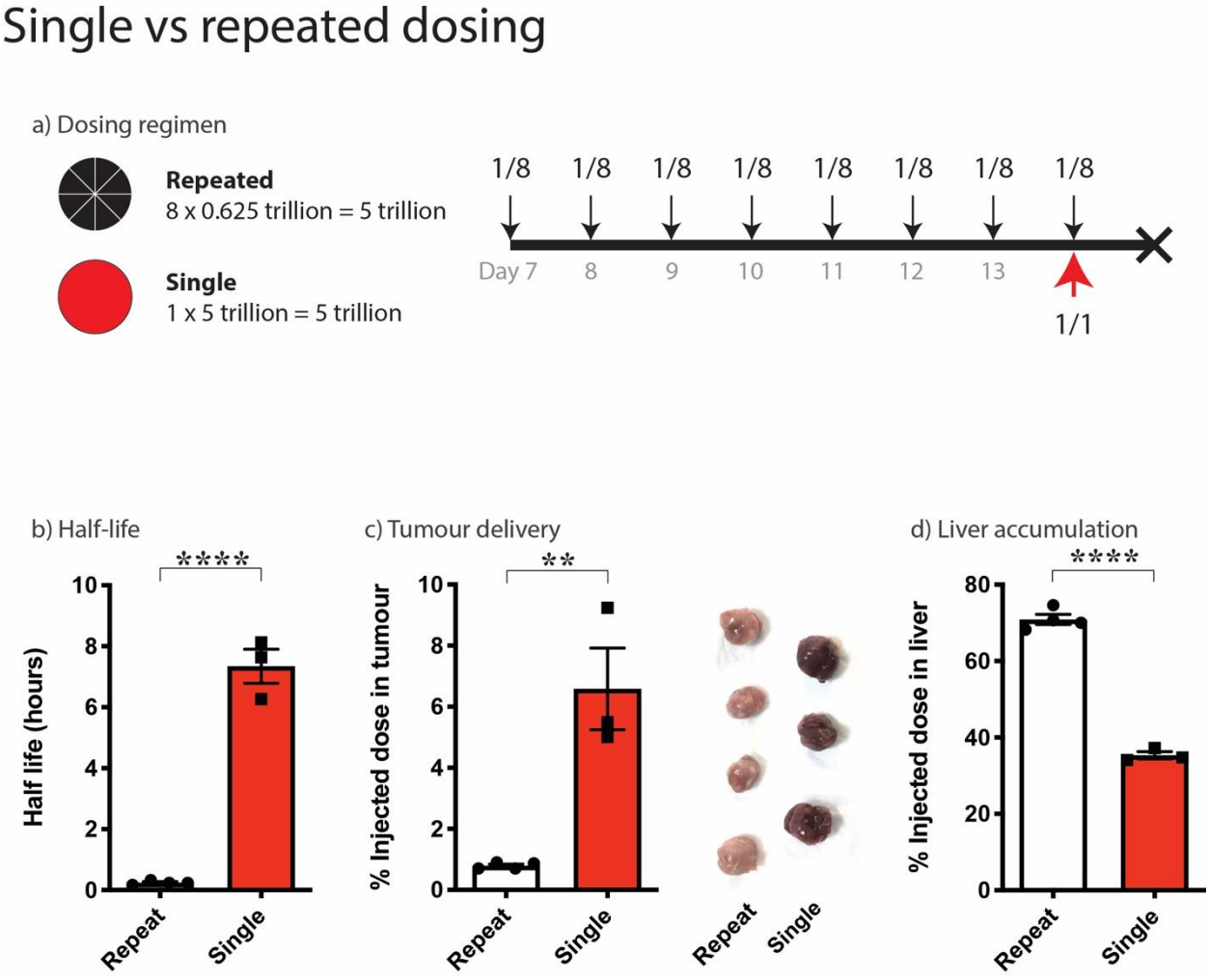


**Supplementary Figure 14 | Single versus repeated dosing**
**(a)** A single dose injection of 5 trillion nanoparticles (above the 1 trillion threshold) into 4T1-tumour bearing BALB/c mice was compared with 8 daily doses of 0.625 trillion nanoparticles (below the 1 trillion threshold). Total dose in both groups was 5 trillion. Mice were inoculated with tumour cells, and 7 days later, were injected daily with 0.625 trillion nanoparticles. On day 14, the single dose group of mice were injected with 5 trillion nanoparticles. On day 15, mice were sacrificed for biodistribution analysis. **(b)** Half-life of bolus doses was longer than that of repeated doses. **(c)** Total tumour delivery of bolus doses was more than that of repeated doses. Gold nanoparticle accumulation in tumours was visible by eye in *ex vivo* tumours (purple). **(d)** Total liver accumulation of bolus doses was less than that of repeated doses. Bars represent mean ± s.e.m. n = 4 for the repeated dose, n = 3 for the single dose. Statistical significance was evaluated using a two-tailed unpaired t-test. ** $p < 0.01$, **** $p < 0.0001$. Exact p-values for (b) $p=2.2x10^{-5}$, (c) $p=0.0035$, (d) $p=6.0x10^{-6}$.

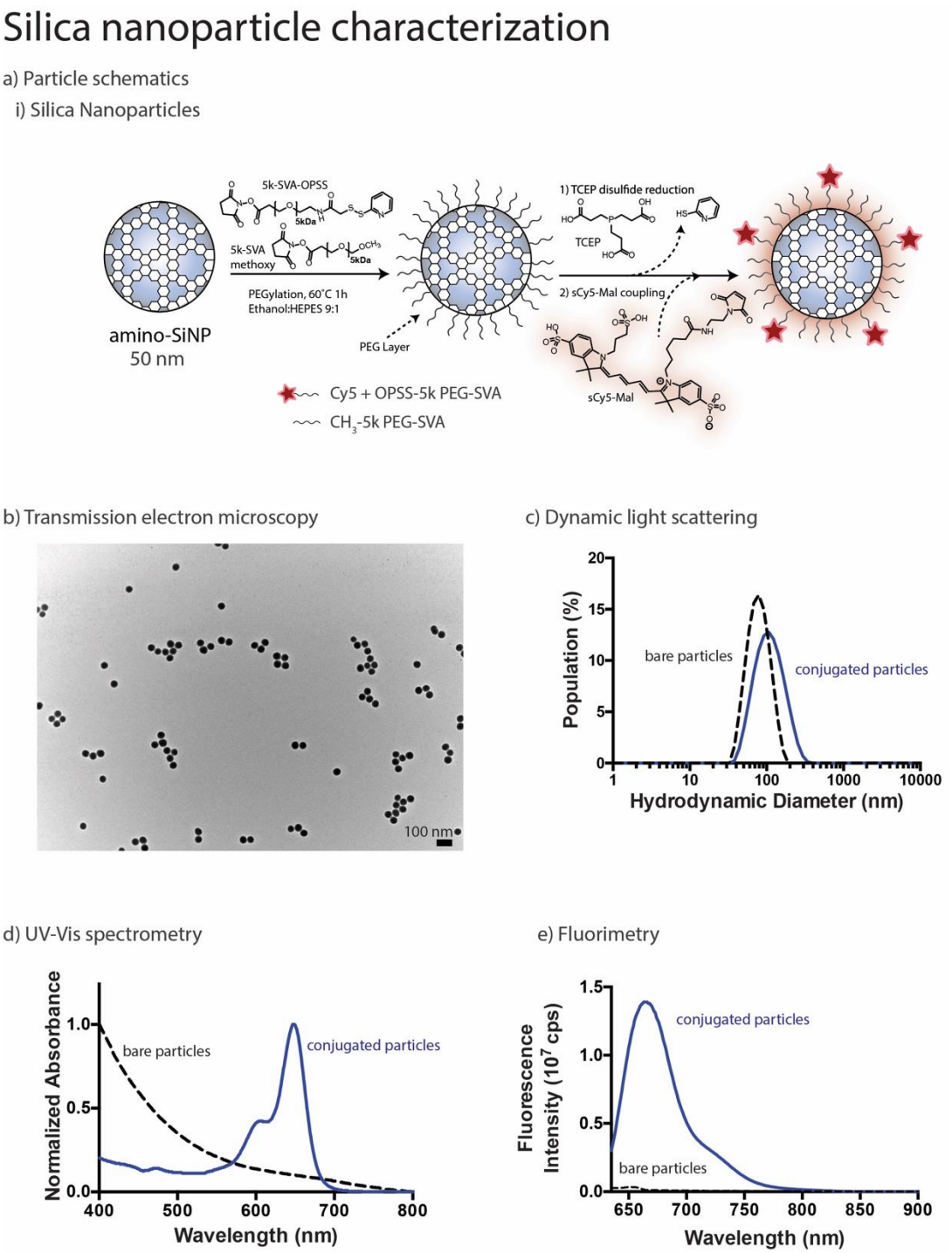


**Supplementary Figure 15 | Silica nanoparticle characterization**
Silica nanoparticles were studied as another inorganic nanoparticle to explore the universality of nonlinear dose responses. **(a)** schematics and synthesis summary of silica nanoparticles. **(b)** Transmission electron microscopy of silica particles 50 nm in diameter. Representative image from n=1 sample from 1 experiment. **(c)** Dynamic light scattering of bare particles and particles conjugated with surface ligands and fluorophores. **(d)** UV-visible spectroscopy of bare silica nanoparticles and silica nanoparticles conjugated with Cy5. **(e)** Fluorescence emission spectra of bare and Cy5-conjugated silica nanoparticles with excitation at 647 nm.

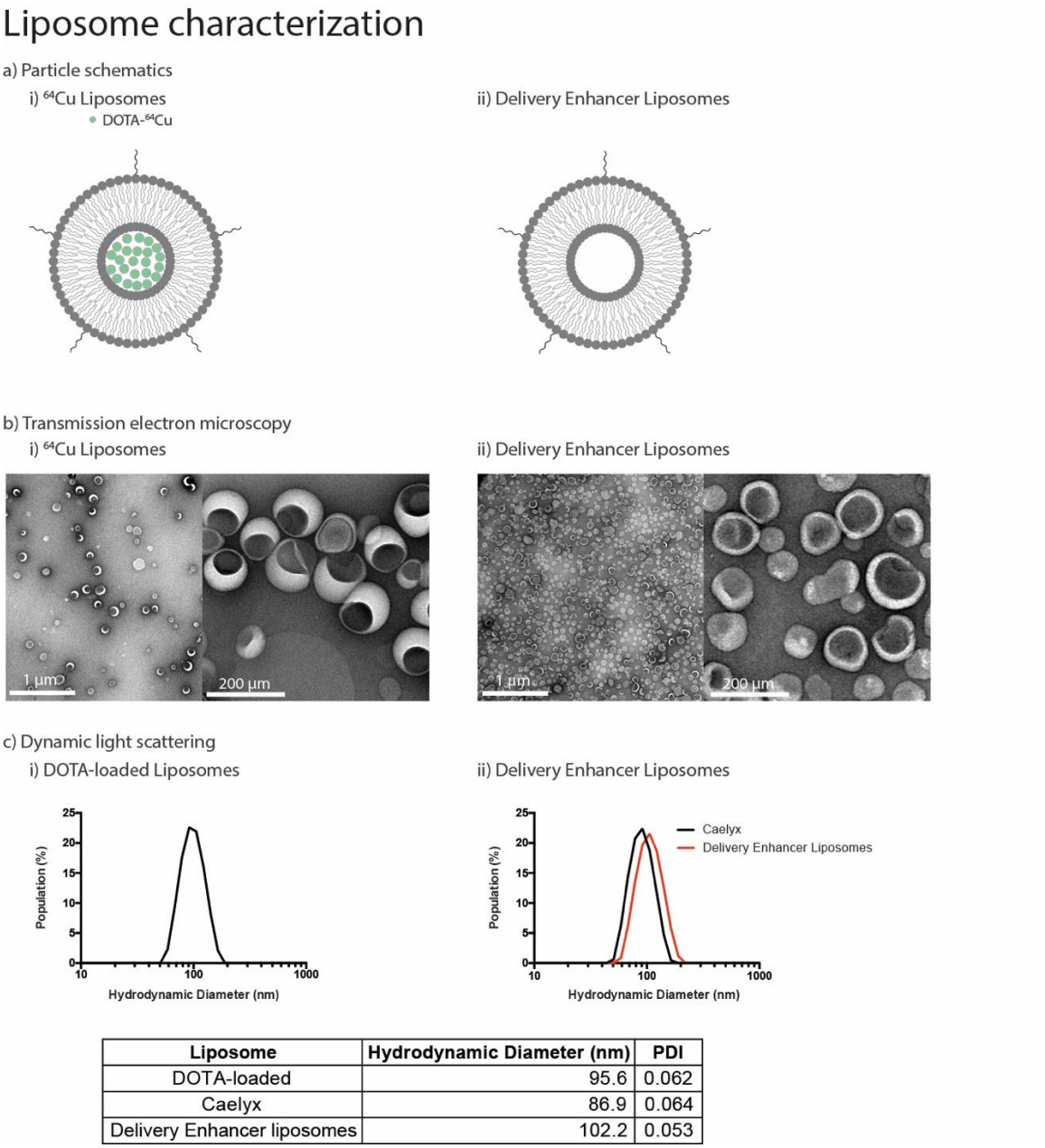


| Liposome | Hydrodynamic Diameter (nm) | PDI |
|---|---|---|
| DOTA-loaded | 95.6 | 0.062 |
| Caelyx | 86.9 | 0.064 |
| Delivery Enhancer liposomes | 102.2 | 0.053 |

**Supplementary Figure 16 | Liposome characterization**
Two types of liposomes were studied as prototypical organic nanoparticles. In the biodistribution experiments, DOTA-$^{64}$Cu-loaded liposomes **(i)** were used to quantify accumulation of liposomes in the liver and tumour. In the therapeutic experiments, Caelyx-similar liposomes without doxorubicin **(ii)** were used to augment the dose of nanoparticles to decrease liver accumulation and increase tumour delivery. **(a)** Schematics of both liposomes. **(b)** Transmission electron microscopy images of liposomes. Liposomes appear monodisperse roughly 100 nm in diameter. Their flattened appearance is due to grid preparation artefacts: the liposome's hydrated cores evaporate and hollow out during grid drying, causing deflation. Representative images from n=1 sample from 1 experiment. **(c)** Dynamic light scattering shows both synthesized liposomes have a hydrodynamic diameter of around 96 nm, consistent with commercial Caelyx, which showed 87 nm.

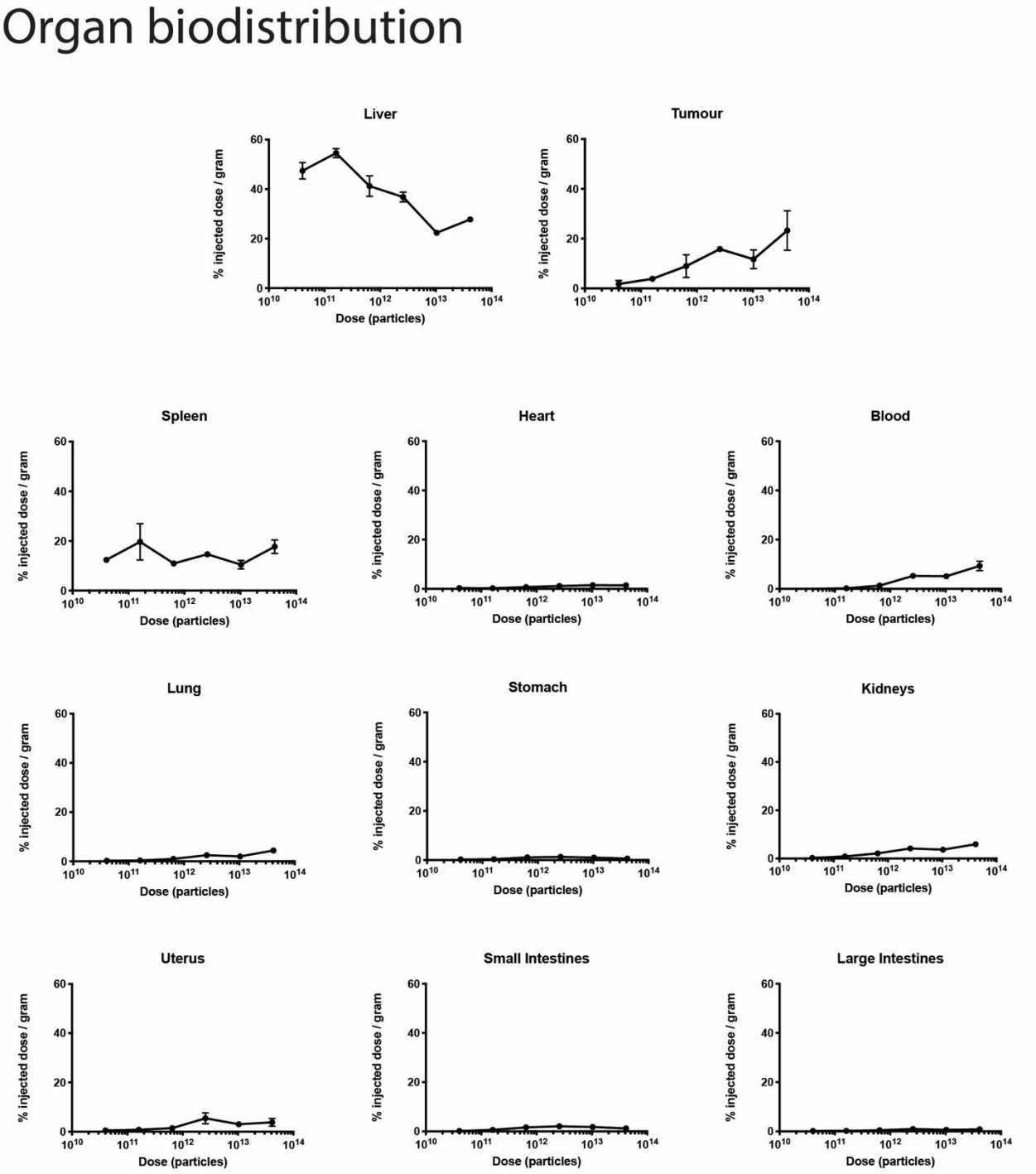


**Supplementary Figure 17 | Biodistribution of 50 nm gold nanoparticles in organs**
Supplemental organs to Figure 3a,b. BALB/c mice with 2-week old 4T1 tumours were injected intravenously with varying doses of 50 nm gold nanoparticles, then sacrificed 24 hours later. Organs were excised and quantified for gold nanoparticle accumulation using ICP-MS. Y-axis was set to a maximum of 60% injected dose / gram, as in Figure 1a. Notably, splenic accumulation was not correlated with dose. n =3. All data points represent mean ± s.e.m.

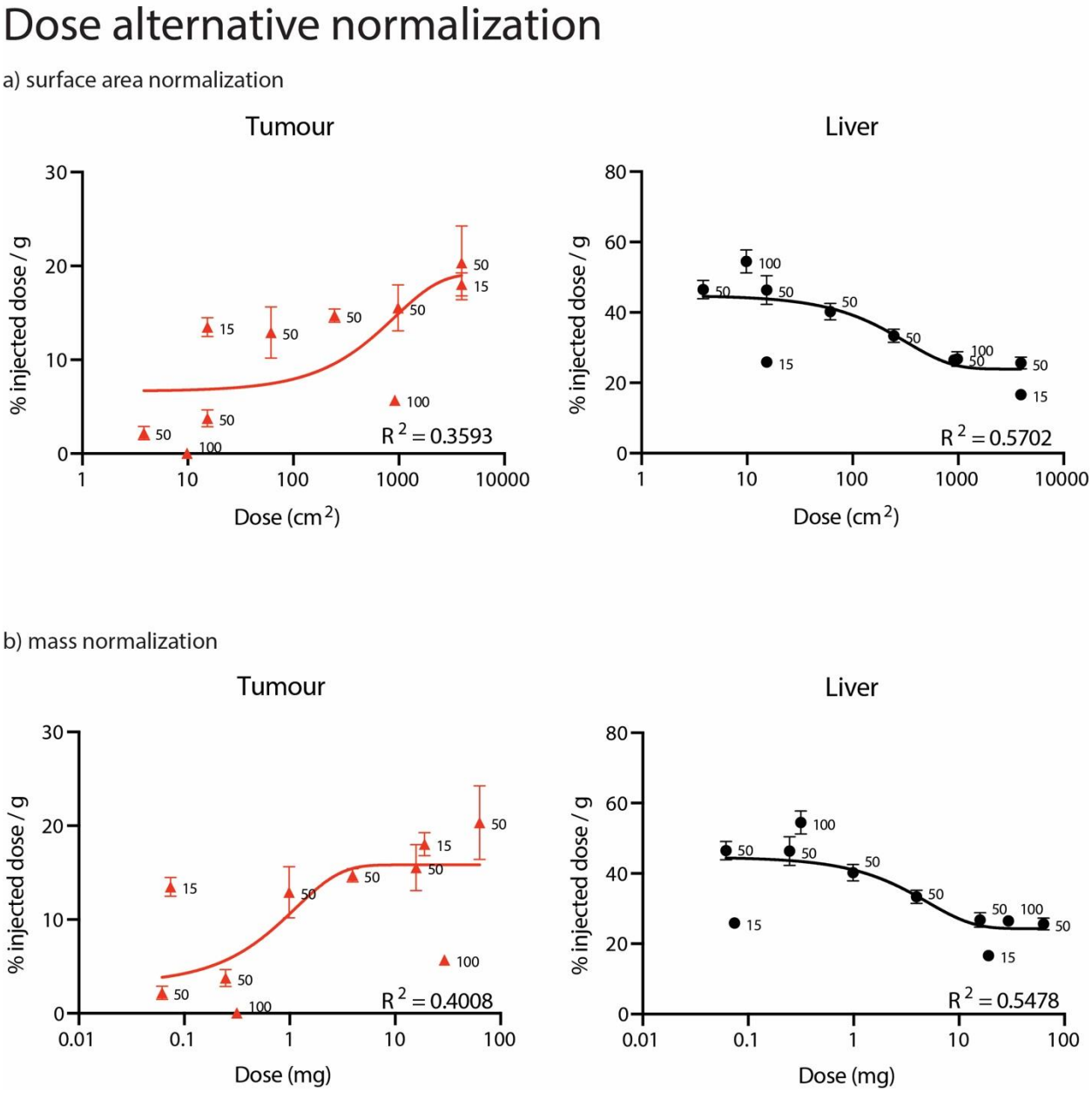


**Supplementary Figure 18 | Dose alternative normalization**
Supplementary figure to Figure 3a,b. **(a)** Dose was renormalized by surface area in $cm^2$ for tumours (left) and livers (right). Correlation between surface area dose and % injected dose / g was lower than correlation between number dose and % injected dose / g. **(b)** Dose was renormalized by mass in mg of gold for tumours (left) and livers (right). Correlation between mass dose and % injected dose / g was lower than correlation between number dose and % injected dose / g. This further confirmed that dose by number of nanoparticles is the most appropriate standard unit for dose. n = 6 for 50 nm nanoparticles and n = 3 for 15 nm and 100 nm nanoparticles. All data points represent mean ± s.e.m.

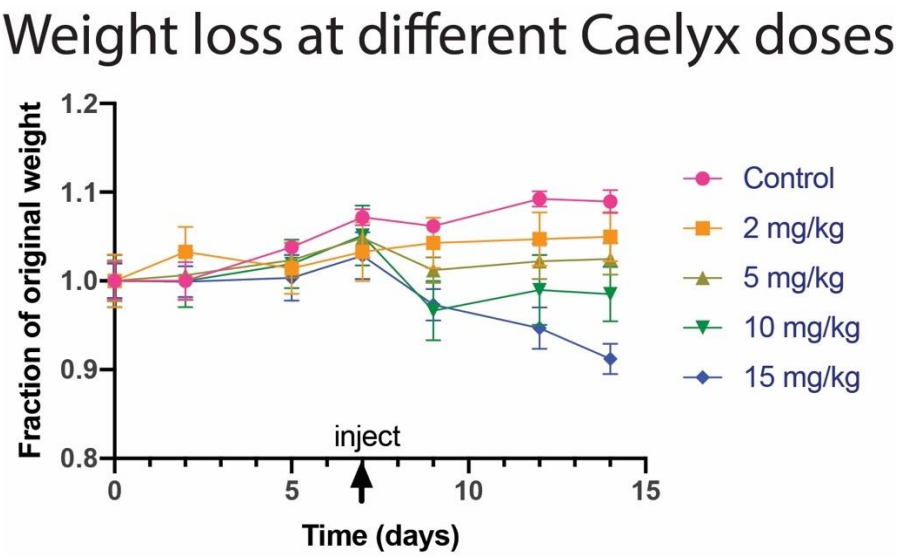


**Supplementary Figure 19 | Effects of Caelyx dose on weight loss in mice**
Mice were given doses of Caelyx nanoparticles between 2-15 mg/kg doxorubicin. Weight responses are shown. Data points represent mean ± s.e.m. of n = 5 mice.

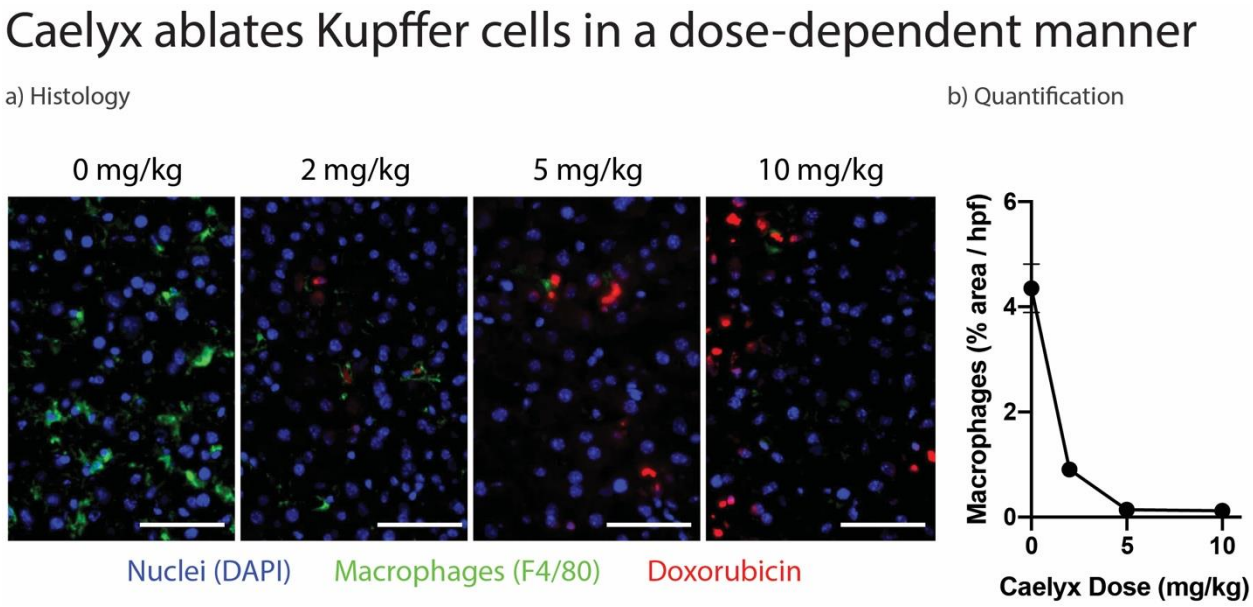


**Supplementary Figure 20 | Caelyx's dose-dependent ablation of Kupffer cells**
**(a)** Representative liver cryosections of mice administered with 0, 2, 5, 10 mg/kg of Caelyx (doxorubicin). Sections were stained for nuclei (blue) and F4/80 (green). Doxorubicin was visualized from intrinsic fluorescence (red). F4/80$^{+}$ macrophage numbers decreased as dose increased. Scale bar: 50 μm. **(b)** Quantification of F4/80$^{+}$ macrophages as a function of dose. Data points represent mean ± s.e.m. of n = 5 mice. Scale bar: 50 μm.

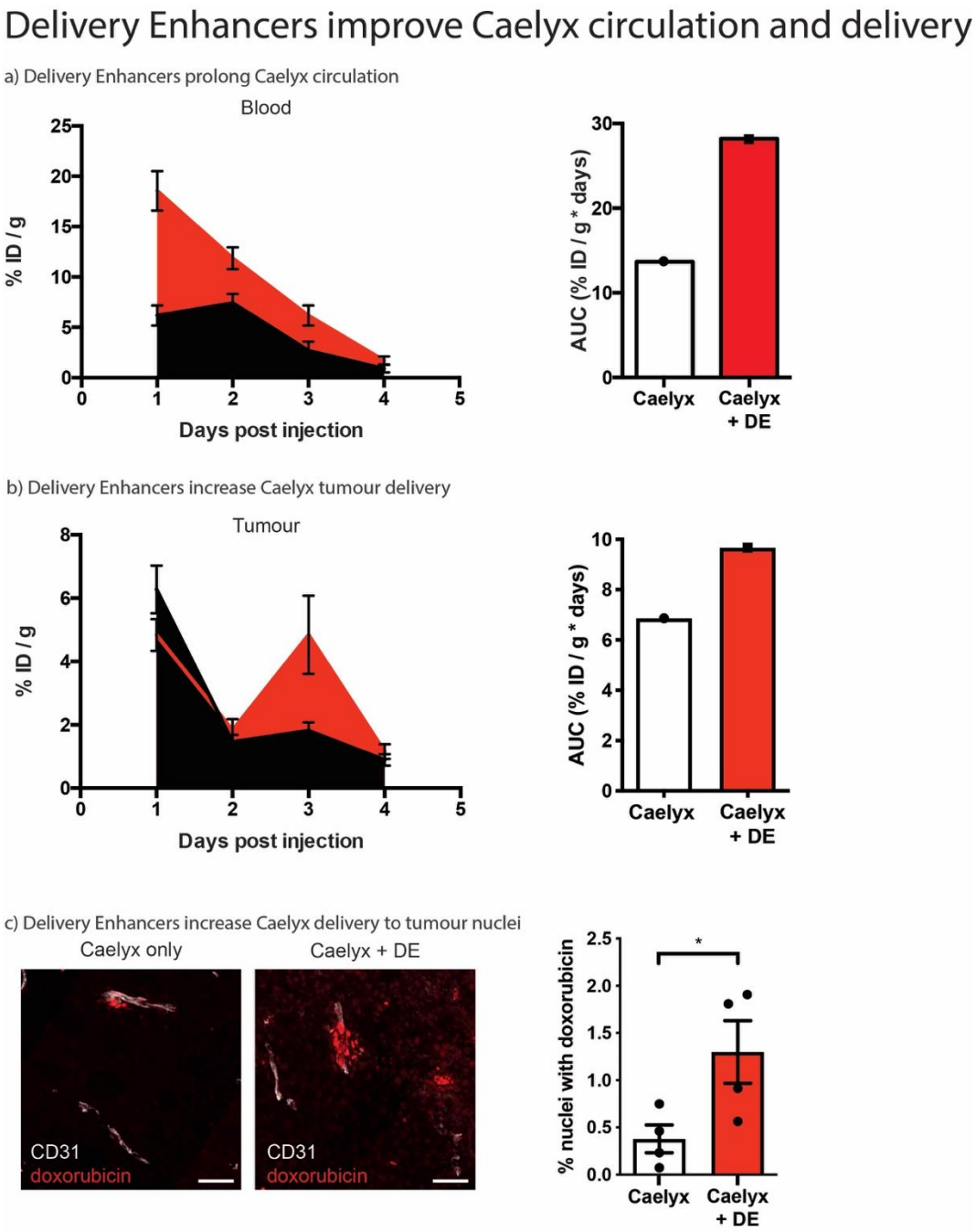


**Supplementary Figure 21 | Caelyx distribution in tissues of mice with delivery enhancers** **(a)** Mice treated with delivery enhancers (red) had greater serum levels of doxorubicin than mice treated without delivery enhancers (black). n = 3 days 1,3; n = 6 days 2,4; error bars represent mean ± s.e.m. Bars on right indicate the area under curve for line plots. n = 1. **(b)** Mice treated with delivery enhancers (red) had greater tumour levels of doxorubicin than mice treated without delivery enhancers (black) n = 3 days 1,3; n = 6 days 2,4; error bars represent mean ± s.e.m. Bars on right indicate the area under curve for line plots. n = 1. **(c)** More tumour nuclei contained doxorubicin in mice treated with delivery enhancers than mice with Caelyx only (n = 4; error bars represent mean ± s.e.m.). Scale bars: 50 μm. Statistical significance was evaluated using a two-tailed unpaired t-test. * $p < 0.05$. Exact p-value for (c) p=0.044.

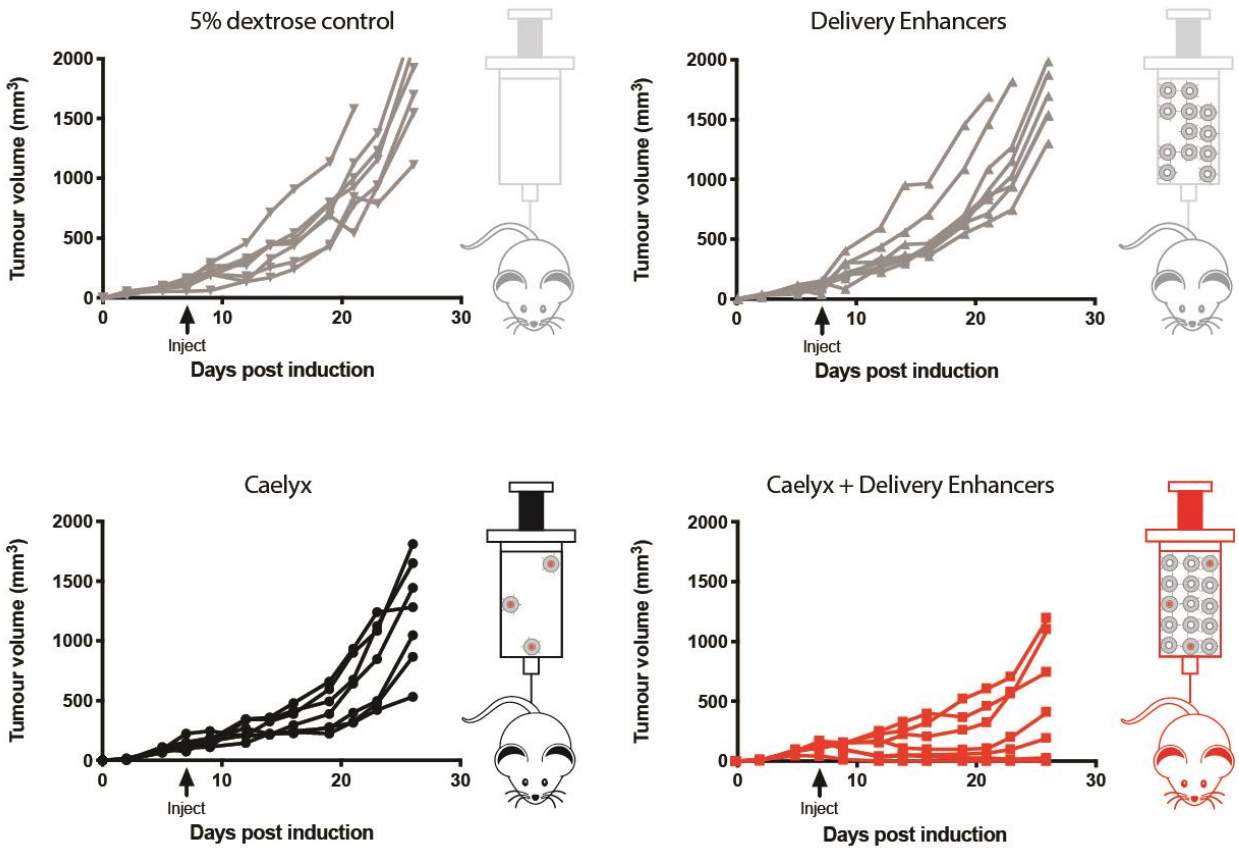


**Supplementary Figure 22 | Growth curves of individual tumours**

Supplementary information for Figure 5b, illustrating individual growth curves of the tumours. n=7 mice for each treatment group.

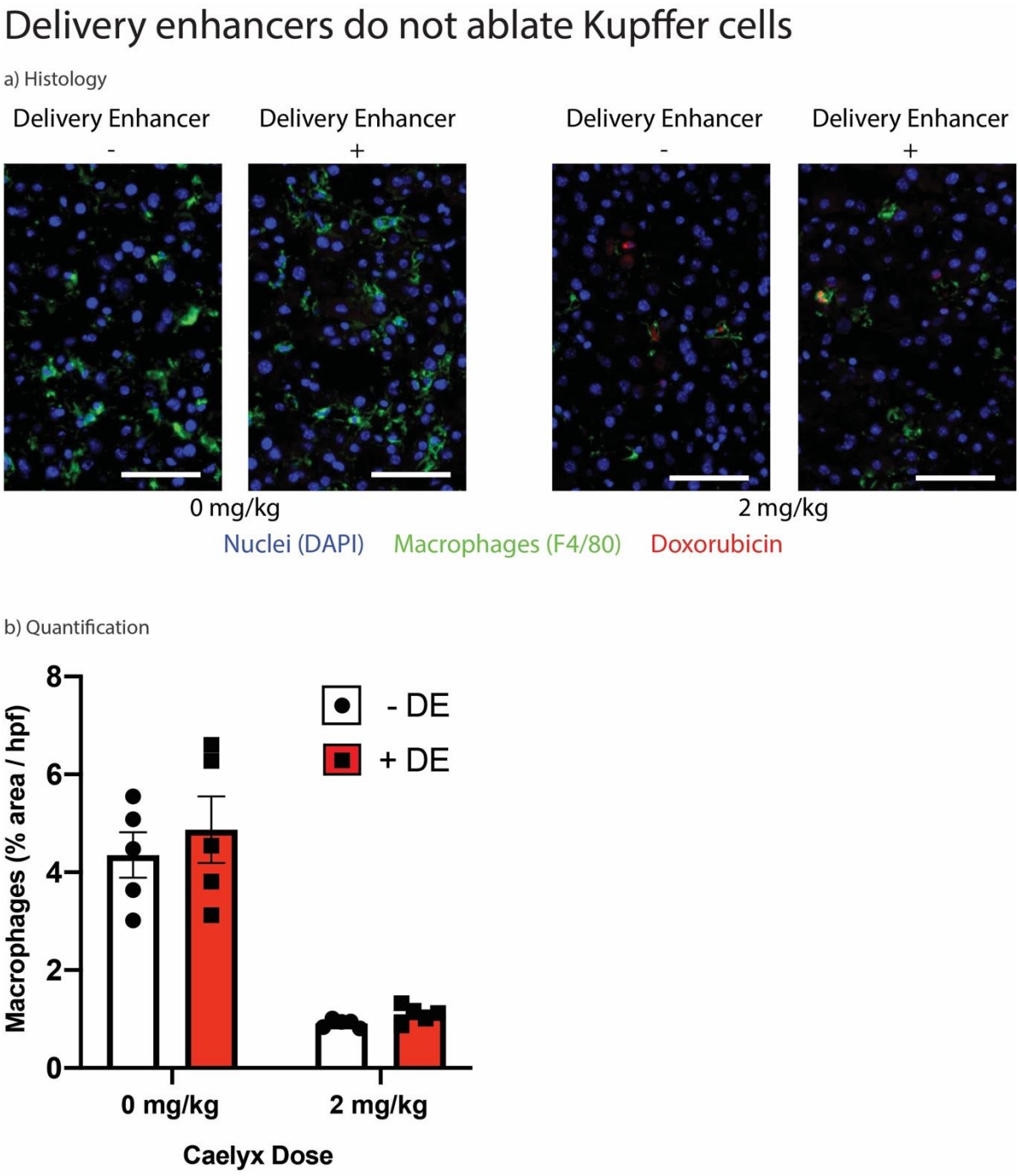


**Supplementary Figure 23 | Delivery enhancers did not ablate Kupffer cell numbers** **(a)** Representative liver cryosections of mice administered with 0 or 2 mg/kg of Caelyx (doxorubicin). Sections were stained for nuclei (blue) and F4/80 (green). Doxorubicin was visualized from intrinsic fluorescence (red). Delivery enhancers did not change the number of $F4/80^+$ macrophages at each Caelyx dose. **(b)** Quantification of $F4/80^+$ macrophages as a function of Caelyx dose and presence of delivery enhancers. Data points represent mean ± s.e.m. of n = 5. Statistical significance was evaluated using a two-tailed unpaired t-test.

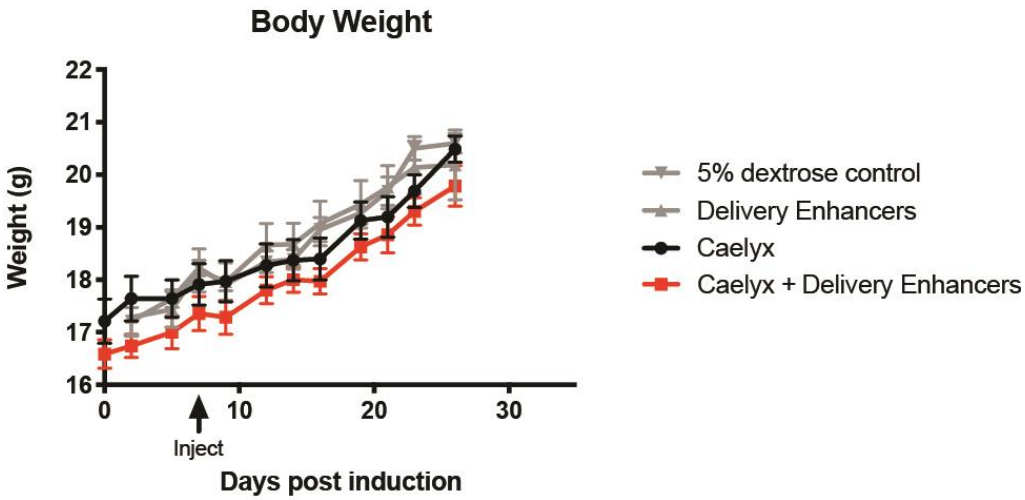


**Supplementary Figure 24 | Mouse body weights**
Mice did not exhibit difference in weight growth between treatment and control groups. All data points and error bars represent the mean ± s.e.m. n = 7 for each treatment group.

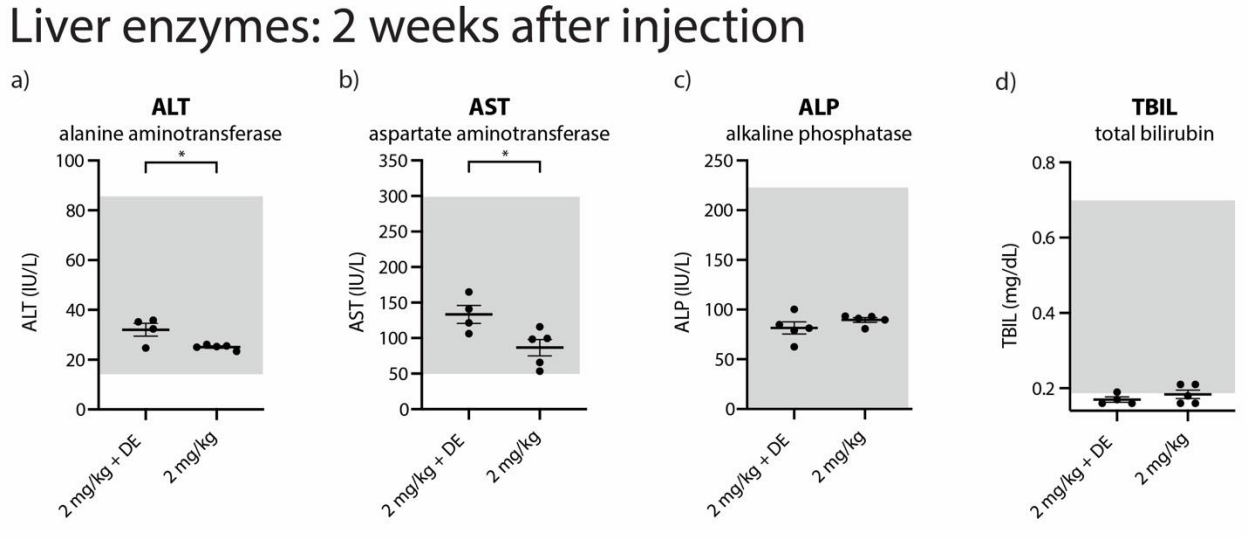


**Supplementary Figure 25 | Liver enzymes 2 weeks after Caelyx injection**
Serum from mice injected with Caelyx (2 mg/kg) with and without delivery enhancers analyzed for **(a)** alanine aminotransferase, **(b)** aspartate aminotransferase, **(c)** alkaline phosphatase, **(d)** and total bilirubin. Lines represent mean ± s.e.m. (n = 5; with exception of ALT and AST in 2 mg/kg + DE group that have n = 4). Grey shading represents physiological reference intervals. Statistical significance was evaluated using a two-tailed unpaired t-test. Exact p-values for (a) 0.020, (b) 0.03, (c) 0.25, (d) 0.36.

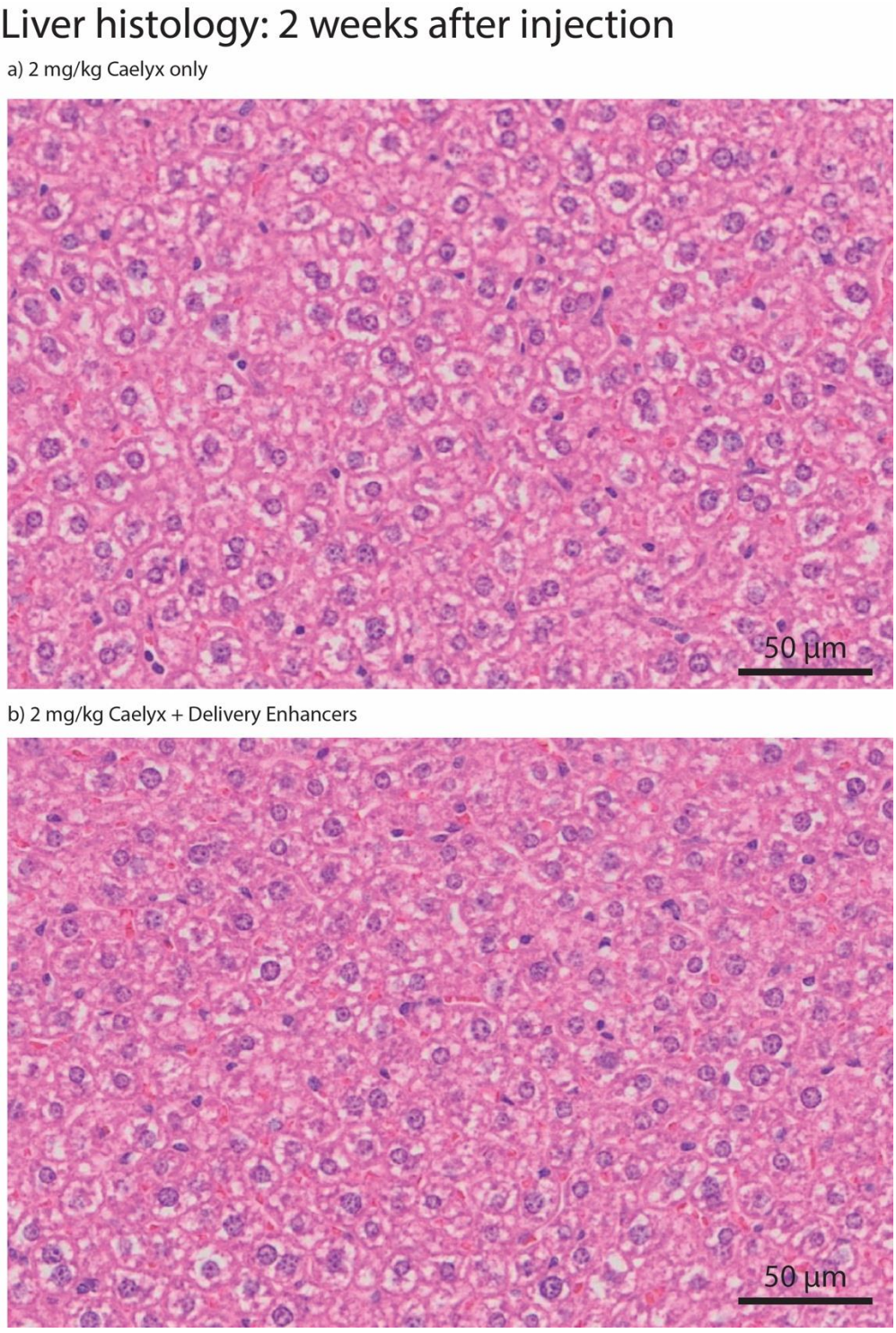


**Supplementary Figure 26 | Liver histology 2 weeks after injection**
**(a)** H&E-stained liver section of a mouse that received Caelyx (2 mg/kg) two weeks prior. **(b)** H&E-stained liver section of a mouse that received Caelyx (2 mg/kg) and delivery enhancers 2 weeks prior. There were no signs of focal necrosis, focal fibrosis, sinusoidal atrophy, and no edema in all groups. Representative images from n=3 animals from 1 experiment.

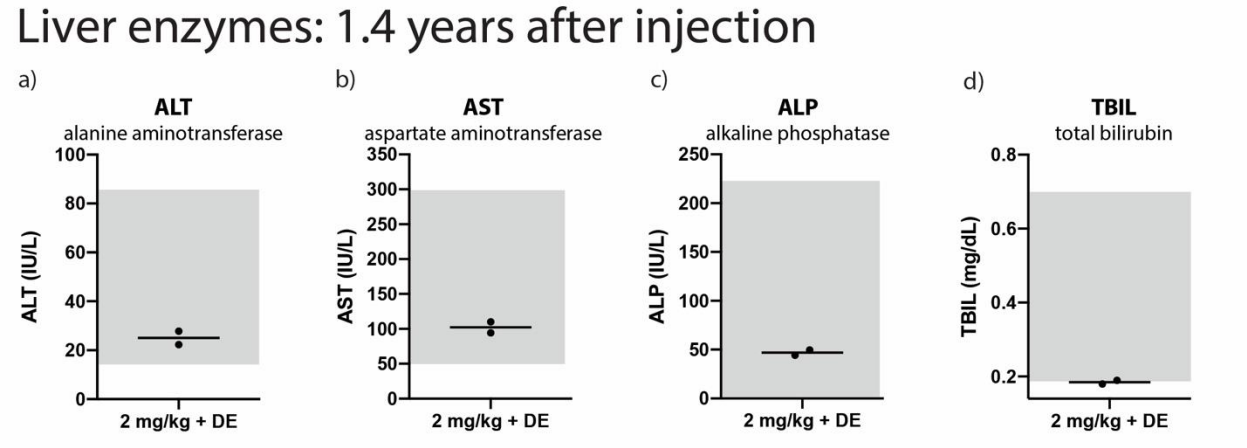


**Supplementary Figure 27 | Liver enzymes 1.4 years after injection**
Serum from mice injected with Caelyx (2 mg/kg) with delivery enhancers analyzed for **(a)** alanine aminotransferase, **(b)** aspartate aminotransferase, **(c)** alkaline phosphatase, **(d)** and total bilirubin. Grey shading represents physiological reference intervals. Lines represent mean. (n = 2).


**Supplementary Figure 28 | Liver histology 1.4 years after injection**
Representative H&E-stained liver section of a mouse that received Caelyx (2 mg/kg) and delivery enhancers 2 weeks prior. There were no signs of focal necrosis, focal fibrosis, sinusoidal atrophy, nor edema in all groups. Representative image from n=2 animals from 1 experiment.

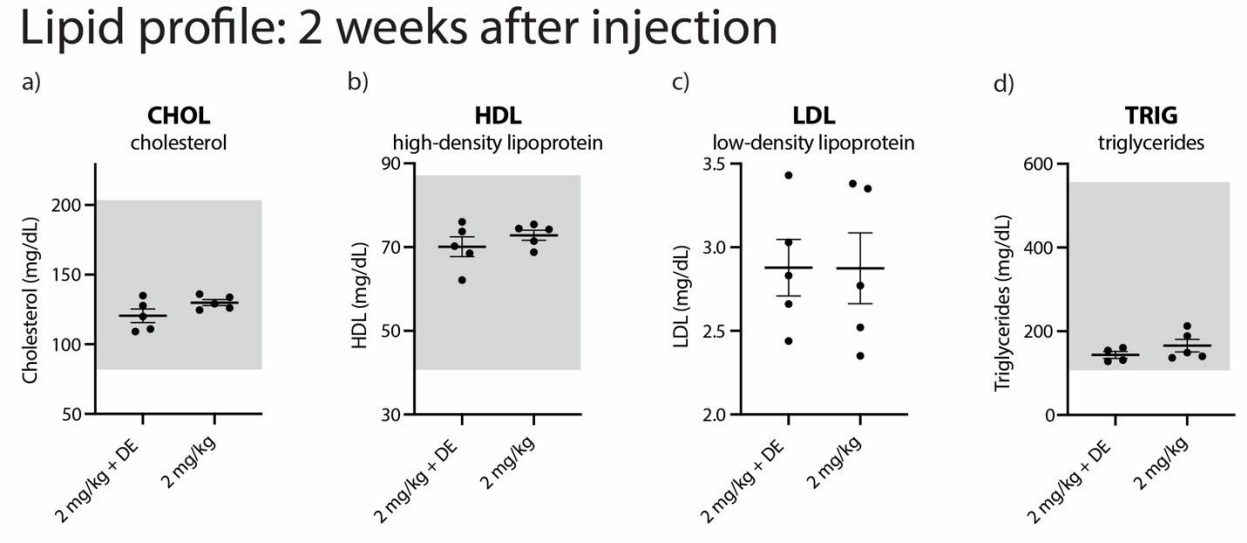


**Supplementary Figure 29 | Lipid profiles 2 weeks after injection**

Serum from mice injected with Caelyx (2 mg/kg) with and without delivery enhancers analyzed for **(a)** cholesterol, **(b)** high-density lipoprotein, **(c)** low-density lipoprotein, **(d)** and triglycerides. Grey shading represents physiological reference intervals. Lines represent mean ± s.e.m. (n = 5). Statistical significance was evaluated using a two-tailed unpaired t-test. Exact p-values for (a) p=0.12, (b) p=0.34, (c) p=0.99, (d) 0.27.

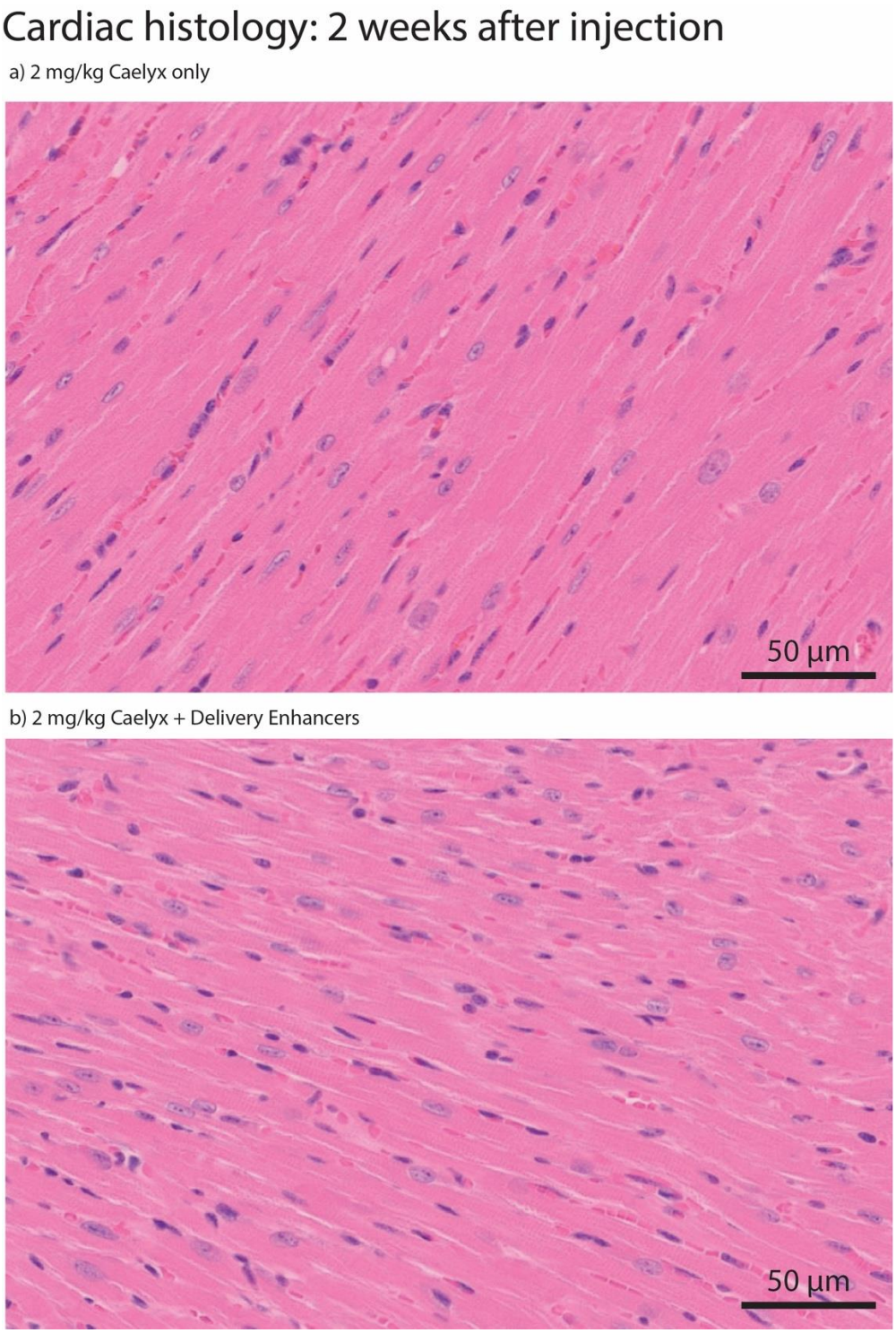


**Supplementary Figure 30 | Cardiac histology 2 weeks after injection**
**(a)** H&E-stained heart section of a mouse that received Caelyx (2 mg/kg) two weeks prior. **(b)** H&E-stained heart section of a mouse that received Caelyx (2 mg/kg) and delivery enhancers 2 weeks prior. There were no signs of polymorphonuclear infiltration, no loss of striated muscle bands, no hemorrhagia, no myocytolysis, and no focal necrosis in all groups. Representative images from n=3 animals from 1 experiment.

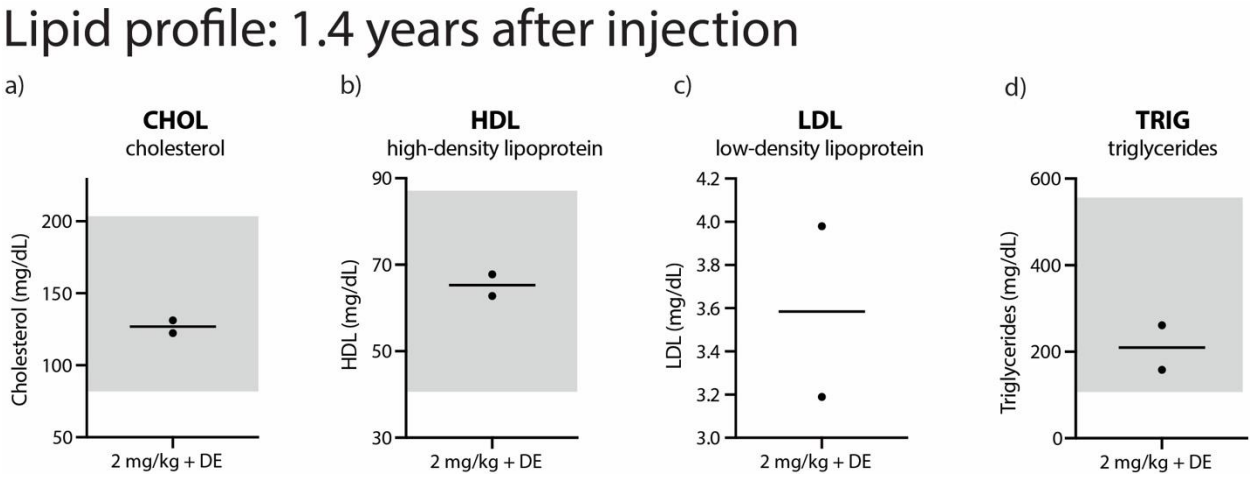


**Supplementary Figure 31 | Lipid profiles 1.4 years after injection**
Serum from mice injected with Caelyx (2 mg/kg) with delivery enhancers analyzed for **(a)** cholesterol, **(b)** high-density lipoprotein, **(c)** low-density lipoprotein, **(d)** and triglycerides. Grey shading represents physiological reference intervals. Lines represent mean. (n = 2).

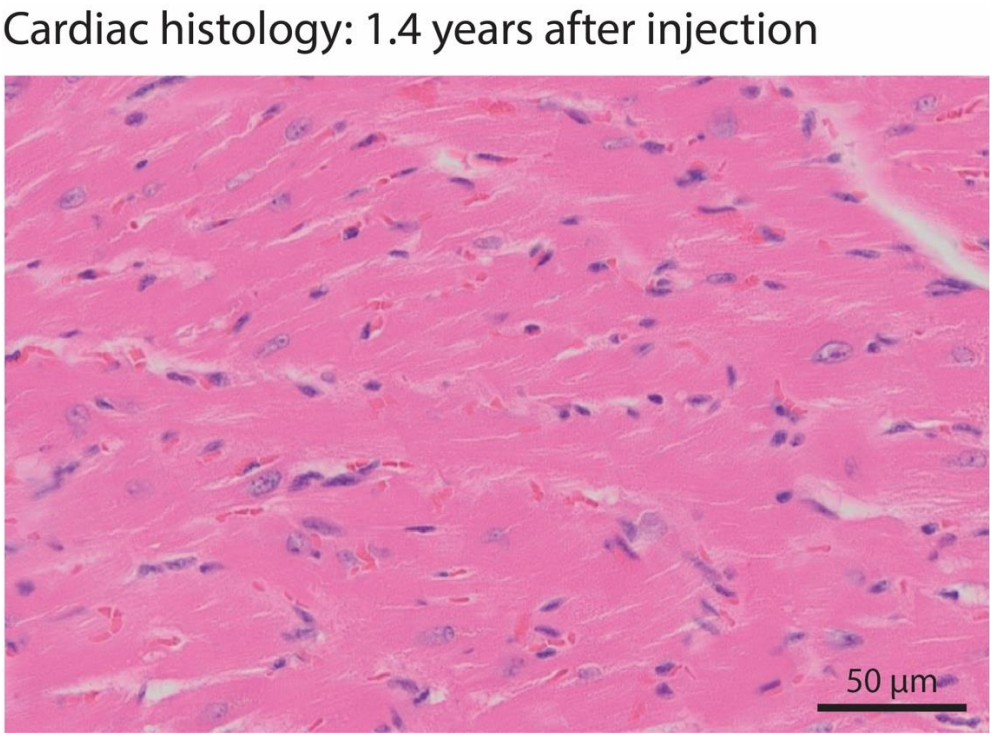


**Supplementary Figure 32 | Cardiac histology 1.4 years after injection**
H&E-stained heart section of a mouse that received Caelyx (2 mg/kg) and delivery enhancers 1.4 years prior. There were no signs of polymorphonuclear infiltration, no loss of striated muscle bands, no hemorrhagia, no myocytolysis, and no focal necrosis. Representative image from n=2 animals from 1 experiment.

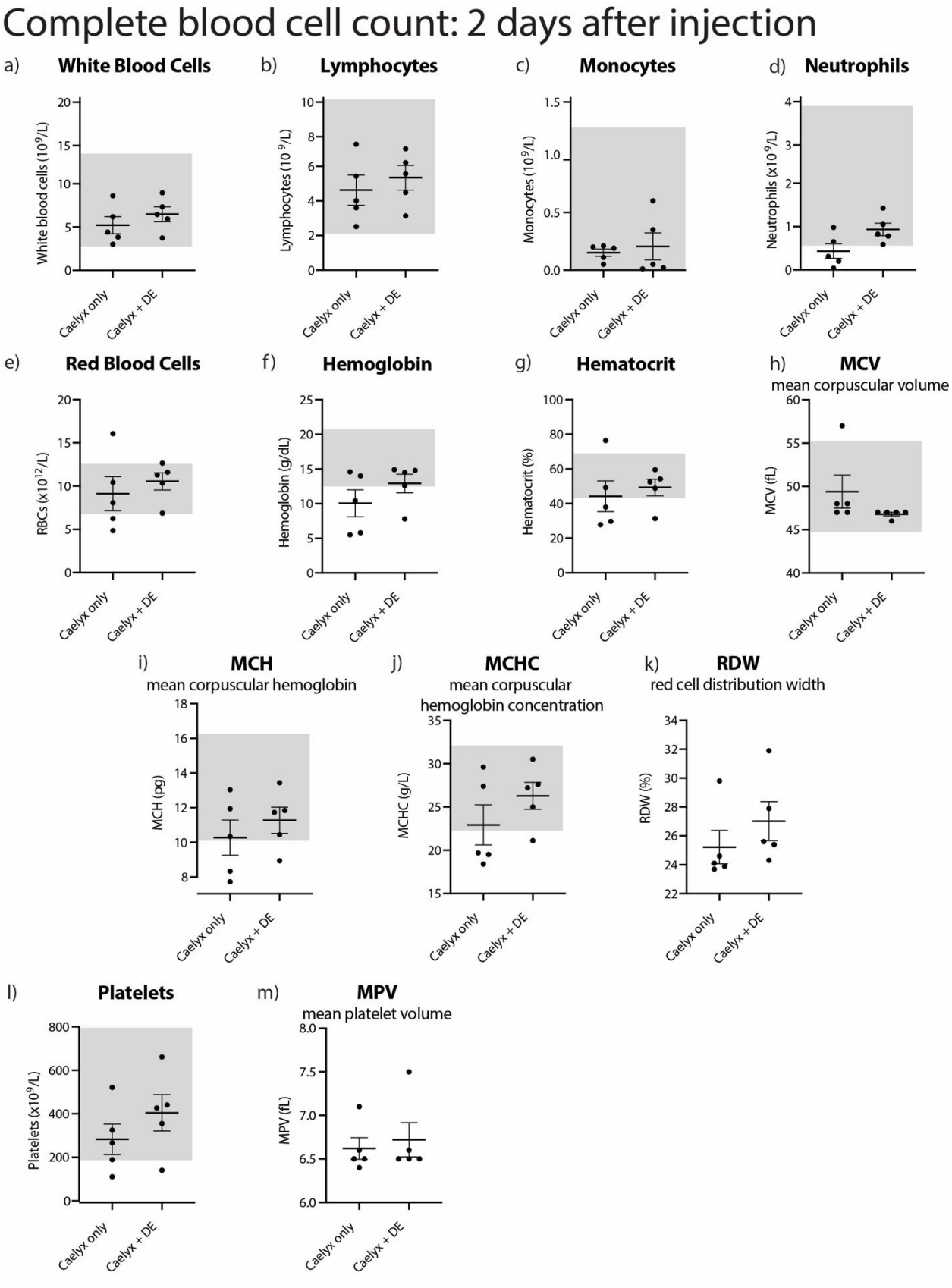
Complete blood cell count: 2 days after injection
a) White Blood Cells
White blood cells (10^9/L)
b) Lymphocytes
Lymphocytes (10^9/L)
c) Monocytes
Monocytes (10^9/L)
d) Neutrophils
Neutrophils (x10^9/L)
e) Red Blood Cells
RBCs (x10^12/L)
f) Hemoglobin
Hemoglobin (g/dL)
g) Hematocrit
Hematocrit (%)
h) MCV
mean corpuscular volume
MCV (fL)
i) MCH
mean corpuscular hemoglobin
MCH (pg)
j) MCHC
mean corpuscular hemoglobin concentration
MCHC (g/L)
k) RDW
red cell distribution width
RDW (%)
l) Platelets
Platelets (x10^9/L)
m) MPV
mean platelet volume
MPV (fL)
Caelyx only
Caelyx + DE

1

**Supplementary Figure 33 | Complete blood cell counts 2 days after injection**
Serum from mice injected with Caelyx (2 mg/kg) with and without delivery enhancers (DE) analyzed for **(a)** white blood cells, **(b)** lymphocytes, **(c)** monocytes, **(d)** neutrophils, **(e)** red blood cells, **(f)** hemoglobin, **(g)** hematocrit, **(h)** mean corpuscular volume, **(i)** mean corpuscular hemoglobin, **(j)** mean corpuscular hemoglobin concentration, **(k)** red cell distribution width, **(l)** platelets, **(m)** mean platelet volume. Although groups did not statistically differ from each other, there were more normal mice in the Caelyx + Delivery Enhancer group. Notably, 3/5 mice that received Caelyx only were neutropenic, compared to 0/5 mice that received Caelyx + Delivery Enhancers, suggesting that delivery enhancers may confer a protective effect from Caelyx's adverse reactions. Grey shading represents physiological reference intervals. Lines represent mean ± s.e.m. n = 5. Statistical significance was evaluated using a two-tailed unpaired t-test. Exact p-values for (a) p=0.36, (b) p=0.54, (c) p=0.67, (d) p=0.054, (e) p=0.54, (f) p=0.26, (g) p=0.63, (h) p=0.21, (i) p=0.45, (j) p=0.26, (k) 0.34, (l) p=0.29, (m) p=0.68.

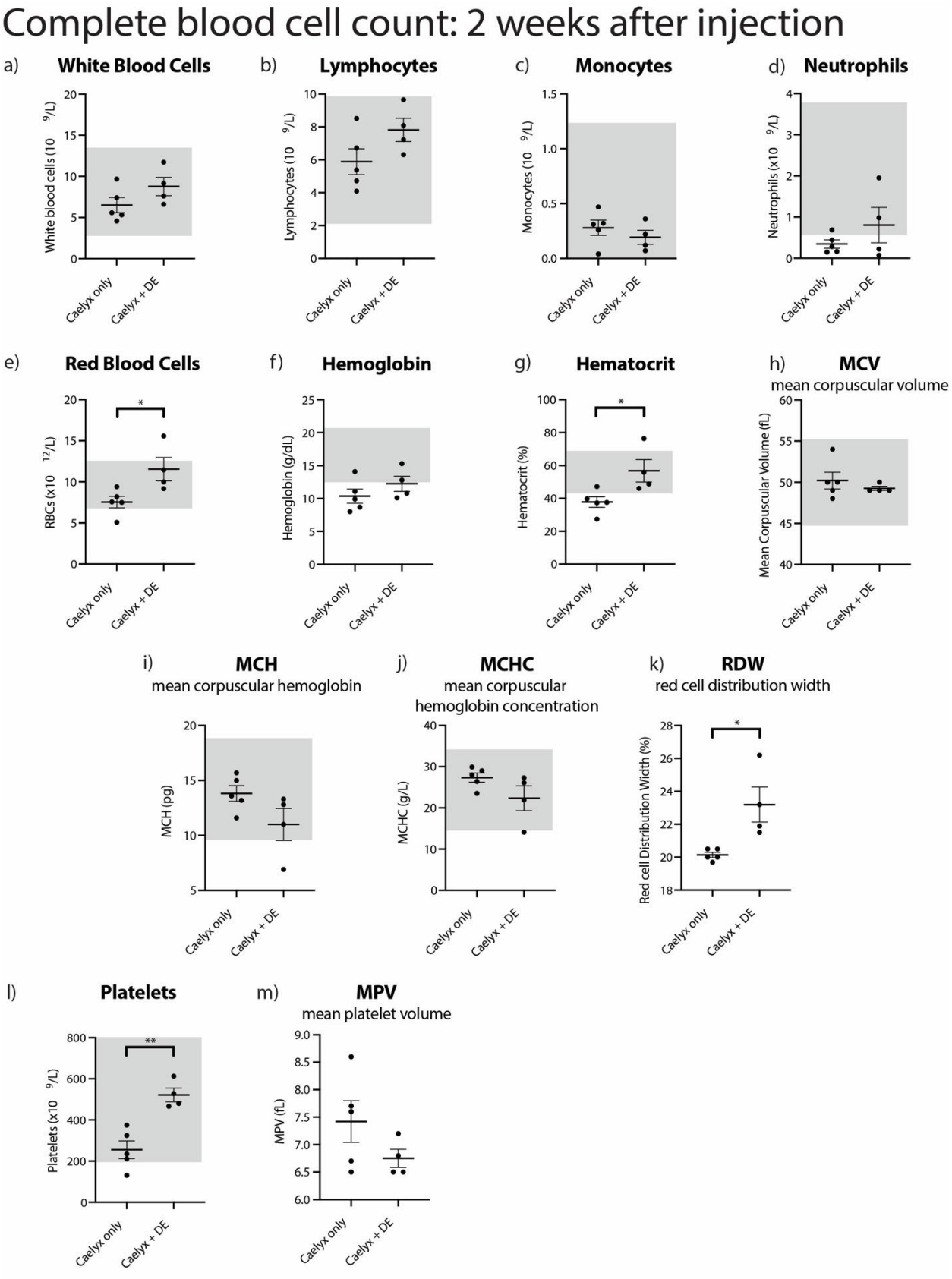
Complete blood cell count: 2 weeks after injection
a) White Blood Cells
White blood cells (10 9/L)
b) Lymphocytes
Lymphocytes (10 9/L)
c) Monocytes
Monocytes (10 9/L)
d) Neutrophils
Neutrophils (x10 9/L)
e) Red Blood Cells
RBCs (x10 12/L)
f) Hemoglobin
Hemoglobin (g/dL)
g) Hematocrit
Hematocrit (%)
h) MCV
mean corpuscular volume
Mean Corpuscular Volume (fL)
i) MCH
mean corpuscular hemoglobin
MCH (pg)
j) MCHC
mean corpuscular hemoglobin concentration
MCHC (g/L)
k) RDW
red cell distribution width
Red cell Distribution Width (%)
l) Platelets
Platelets (x10 9/L)
m) MPV
mean platelet volume
MPV (fL)
Caelyx only
Caelyx + DE

**Supplementary Figure 34 | Complete blood cell counts 2 weeks after injection**
Serum from mice injected with Caelyx (2 mg/kg) with and without delivery enhancers (DE) analyzed for **(a)** white blood cells, **(b)** lymphocytes, **(c)** monocytes, **(d)** neutrophils, **(e)** red blood cells, **(f)** hemoglobin, **(g)** hematocrit, **(h)** mean corpuscular volume, **(i)** mean corpuscular hemoglobin, **(j)** mean corpuscular hemoglobin concentration, **(k)** red cell distribution width, **(l)** platelets, **(m)** mean platelet volume. Notably, mice that received Caelyx only trended towards neutropenia, anemia, and thrombocytopenia, compared to mice that received Caelyx + delivery enhancers, suggesting the delivery enhancers may confer a protective effect against Caelyx's adverse reactions. Grey shading represents physiological reference intervals. Lines represent mean ± s.e.m. n = 5 Caelyx only, n = 4 Caelyx + DE. Statistical significance was evaluated using a two-tailed unpaired t-test. * $p < 0.05$. Exact p-values for (a) p=0.16, (b) p=0.12, (c) p=0.40, (d) p=0.28, (e) p=0.031, (f) p=0.27, (g) p=0.030, (h) p=0.45, (i) p=0.10, (j) p=0.13, (k) 0.015, (l) p=0.002, (m) p=0.18.

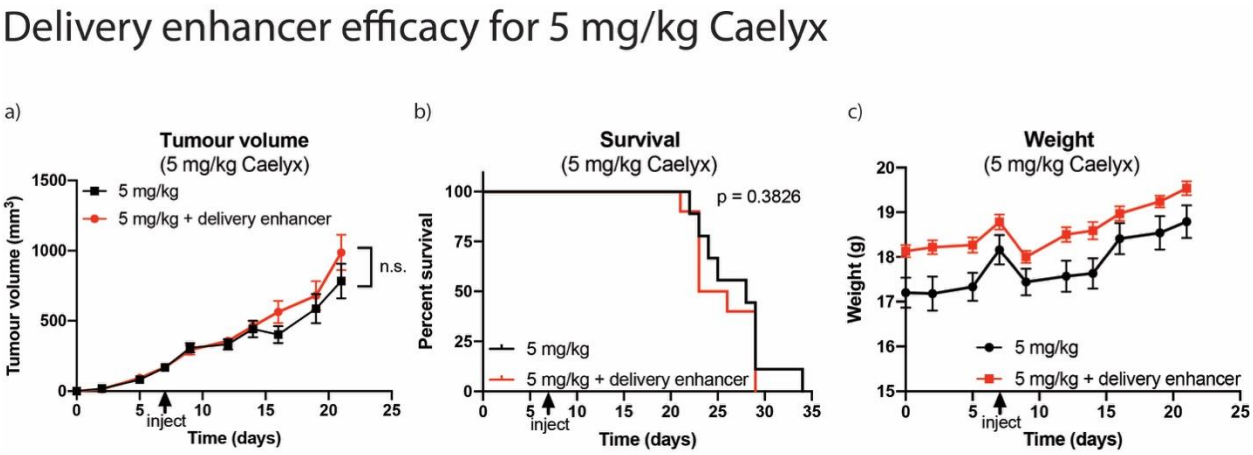


**Supplementary Figure 35 | Delivery enhancers at 5 mg/kg Caelyx**
**(a)** Tumour volumes of mice that received 5 mg/kg Caelyx (12 trillion) with or without delivery enhancers (46 trillion). Data points represent mean ± s.e.m (n = 9). Statistical significance was evaluated using a two-way ANOVA with multiple comparisons with Bonferroni adjustment. Mice were injected 7 days after 4T1 tumour induction. **(b)** Survival of treated mice. Statistical significance was evaluated using a two-tailed Mantel-Cox log-rank test, p = 0.38. **(c)** Weights of treated mice. Data points represent mean ± s.e.m (n = 9).

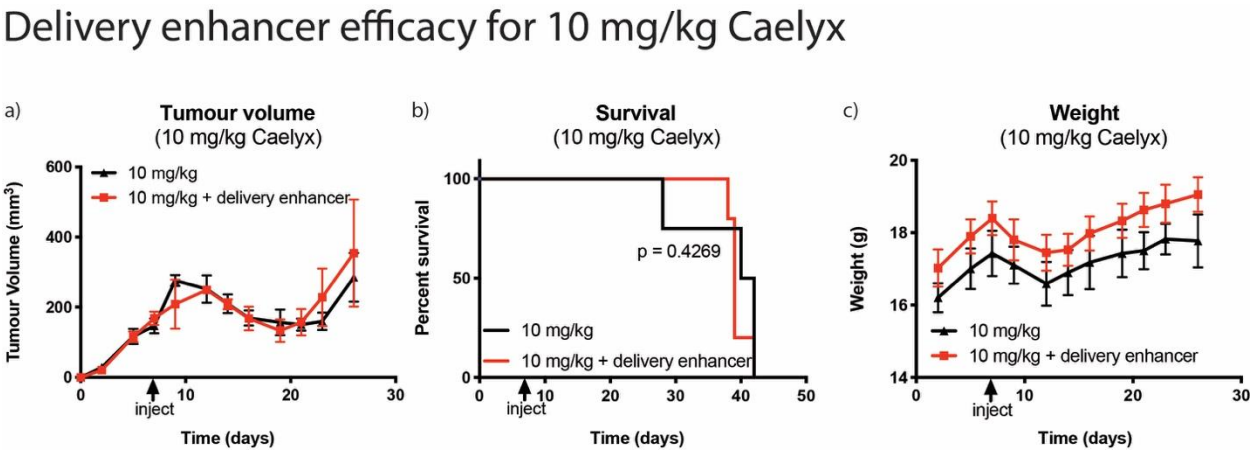


**Supplementary Figure 36 | Delivery enhancers at 10 mg/kg Caelyx**
**(a)** Tumour volumes of mice that received 10 mg/kg Caelyx (23 trillion) with or without delivery enhancers (46 trillion). Data points represent mean ± s.e.m (n = 4). Statistical significance was evaluated using a two-way ANOVA with multiple comparisons with Bonferroni adjustment. Mice were injected 7 days after 4T1 tumour induction. **(b)** Survival of treated mice. Statistical significance was evaluated using a two-tailed Mantel-Cox log-rank test, p = 0.43. **(c)** Weights of treated mice. Data points represent mean ± s.e.m (n = 4).

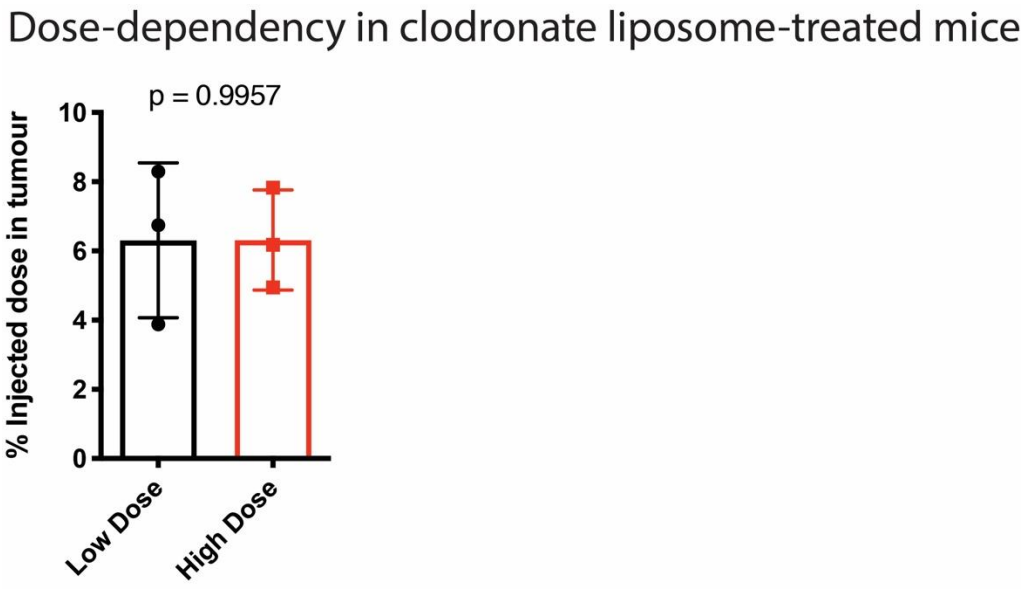


**Supplementary Figure 37 | Dose-dependency in Kupffer cell depleted mice**
Mice were pre-treated with clodronate liposomes 2 days before gold nanoparticle injection (50 nm) to deplete Kupffer cells. Tumour delivery was measured 24 hours after gold nanoparticle injection. Low dose, 0.2 trillion; high dose, 50 trillion. Bars represent mean ± s.e.m. n = 3. Statistical significance was evaluated using a two-tailed unpaired t-test. p=1.

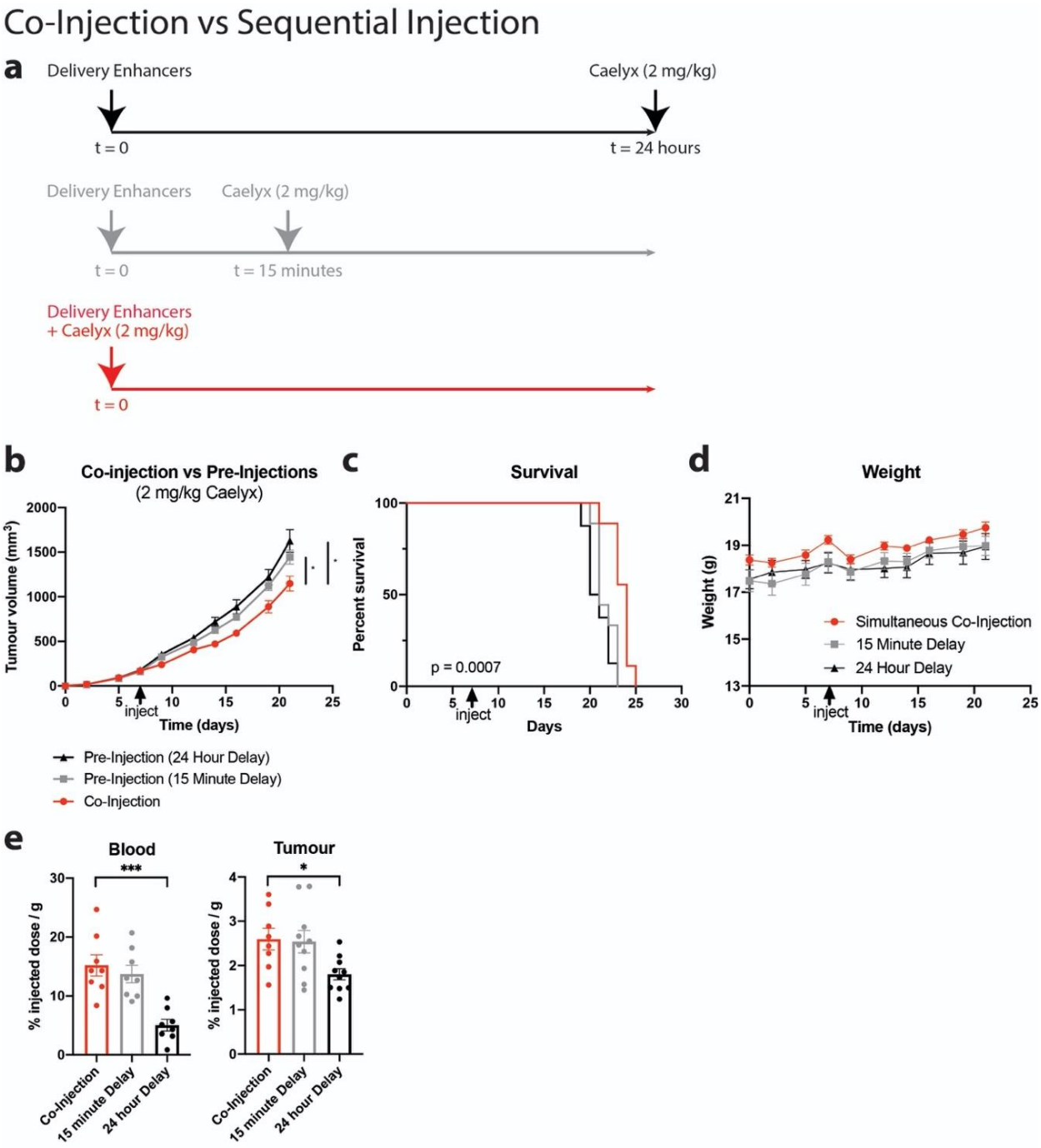


**Supplementary Figure 38 | Co-injection vs. pre-injection of delivery enhancers**
Supplement to Figure 5. **(a)** Timeline of injections. Delivery enhancers (46 trillion) were given with, or before Caelyx (4.6 trillion). Mice were separated into 3 groups: co-injection (red), 15 minute delay (gray), or 24 hour delay (black). **(b)** Tumour volumes of treated mice. Data points represent mean ± s.e.m. Statistical significance was evaluated using a two-way ANOVA with multiple comparisons with Bonferroni adjustment. * $p < 0.05$. Mice were injected 7 days after 4T1 tumour induction. **(c)** Survival of treated mice. Statistical significance was evaluated using a two-tailed Mantel-Cox log-rank test. Post-hoc analyses: co-injection vs 24 hour delay: p =

0.0008, co-injection vs 15 minute delay: p = 0.003. **(d)** Weights of treated mice. **(e)** Blood and tumour doxorubicin quantity 3 days after Caelyx injection. All data represent mean ± s.e.m. (b-d) n=9 co-injection, n=9 pre-injection (15 minute delay), n=8 pre-injection (24 hour delay). (e) n=8. Statistical significance was evaluated using a one-way ANOVA. * $p < 0.05$, *** $p < 0.001$. Exact p-values for (b) co-injection vs 24 hour delay p=0.014, co-injection vs 15 minute delay p = 0.036), (c) p=0.0007, (d) co-injection vs 24 hour delay p=0.39, co-injection vs 15 minute delay p=0.26, (e) blood co-injection vs 24 hour delay p=0.00015, blood co-injection vs 15 minute delay p=0.95; tumour co-injection vs 24 hour delay p=0.029, tumour co-injection vs 15 minute delay p=0.97.

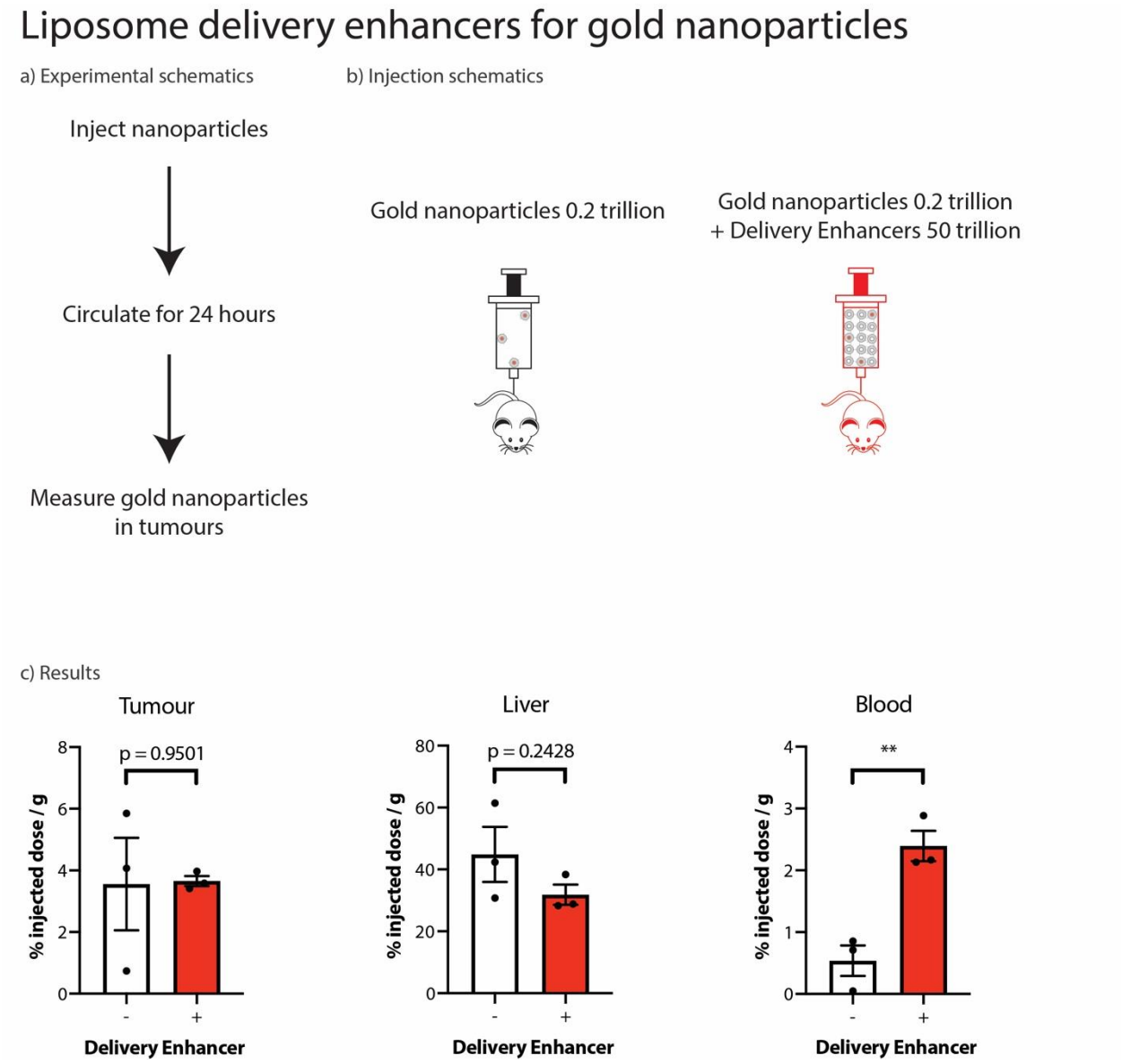


**Supplementary Figure 39 | Specificity of dose enhancement**
Delivery enhancers (46 trillion) were co-injected with a low dose (0.2 trillion) of gold nanoparticles to investigate if dose enhancement required nanoparticle specificity. **(a)** experimental schematics. **(b)** Two groups were investigated: low dose of gold nanoparticles alone versus low dose of gold nanoparticles with delivery enhancers. **(c)** The tumour and liver were not statistically different in their accumulation of gold nanoparticles. The amount of nanoparticles remaining in endpoint blood at 24 hours was statistically different (** $p < 0.01$). Data points represent mean ± s.e.m (n = 3). Statistical significance was evaluated using a two-tailed unpaired t-test. Exact p-values for (c) tumour p=0.95, liver p=0.24, blood p=0.0060.

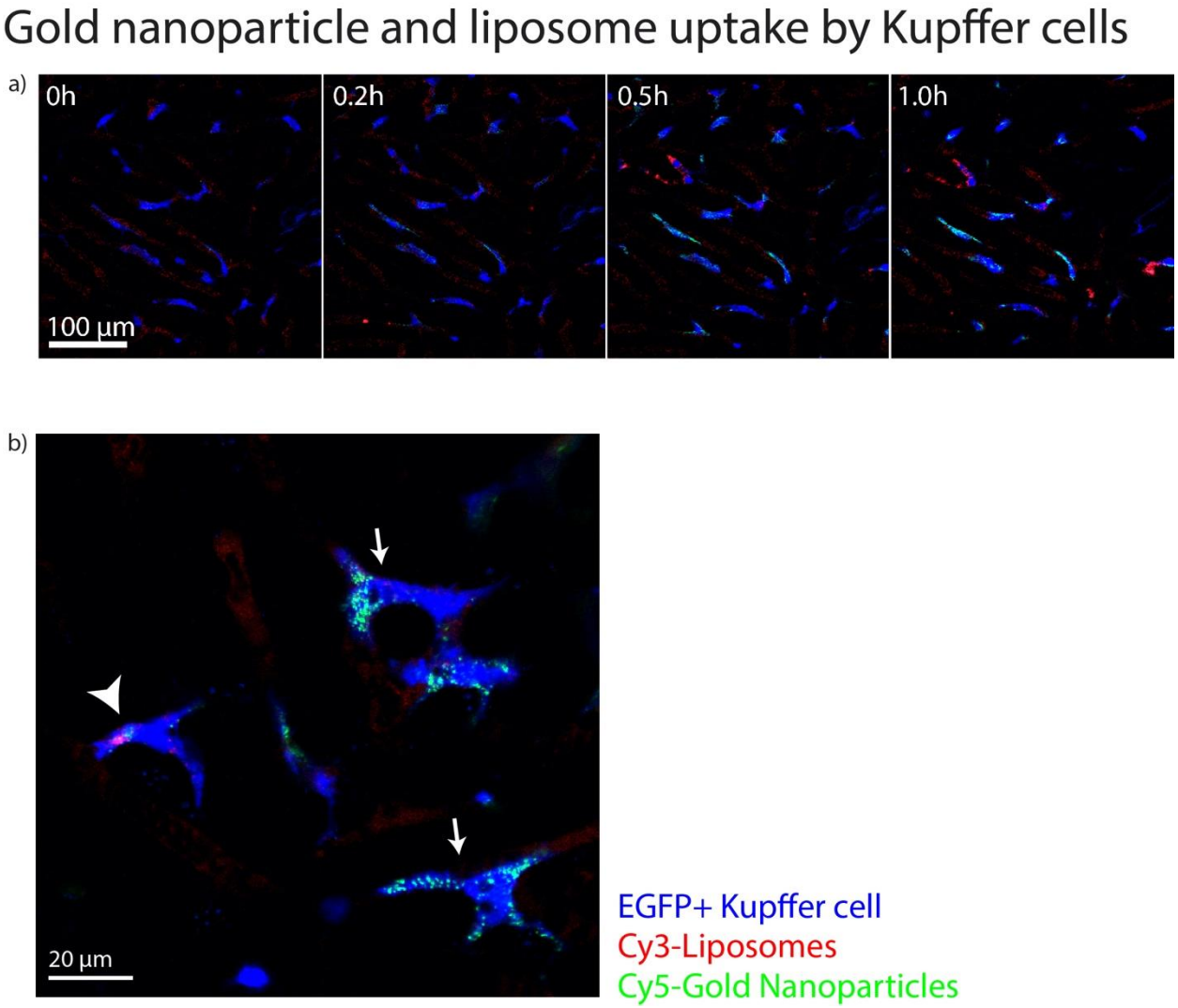


**Supplementary Figure 40 | Gold nanoparticle and liposome uptake by Kupffer cells** Intravital liver imaging depicting single-cell images of live Kupffer cells *in vivo*. **(a)** Timelapse uptake of liposomes (red) and gold nanoparticles (green) in Kupffer cells (blue) over 1 hour. **(b)** Higher magnification of live Kupffer cells *in vivo* at 1 hour after injection demonstrating that some Kupffer cells predominantly take up liposomes (arrowhead) and some Kupffer cells take up only gold nanoparticles (arrows). Representative images from n=3 animals from 3 independent experiments.

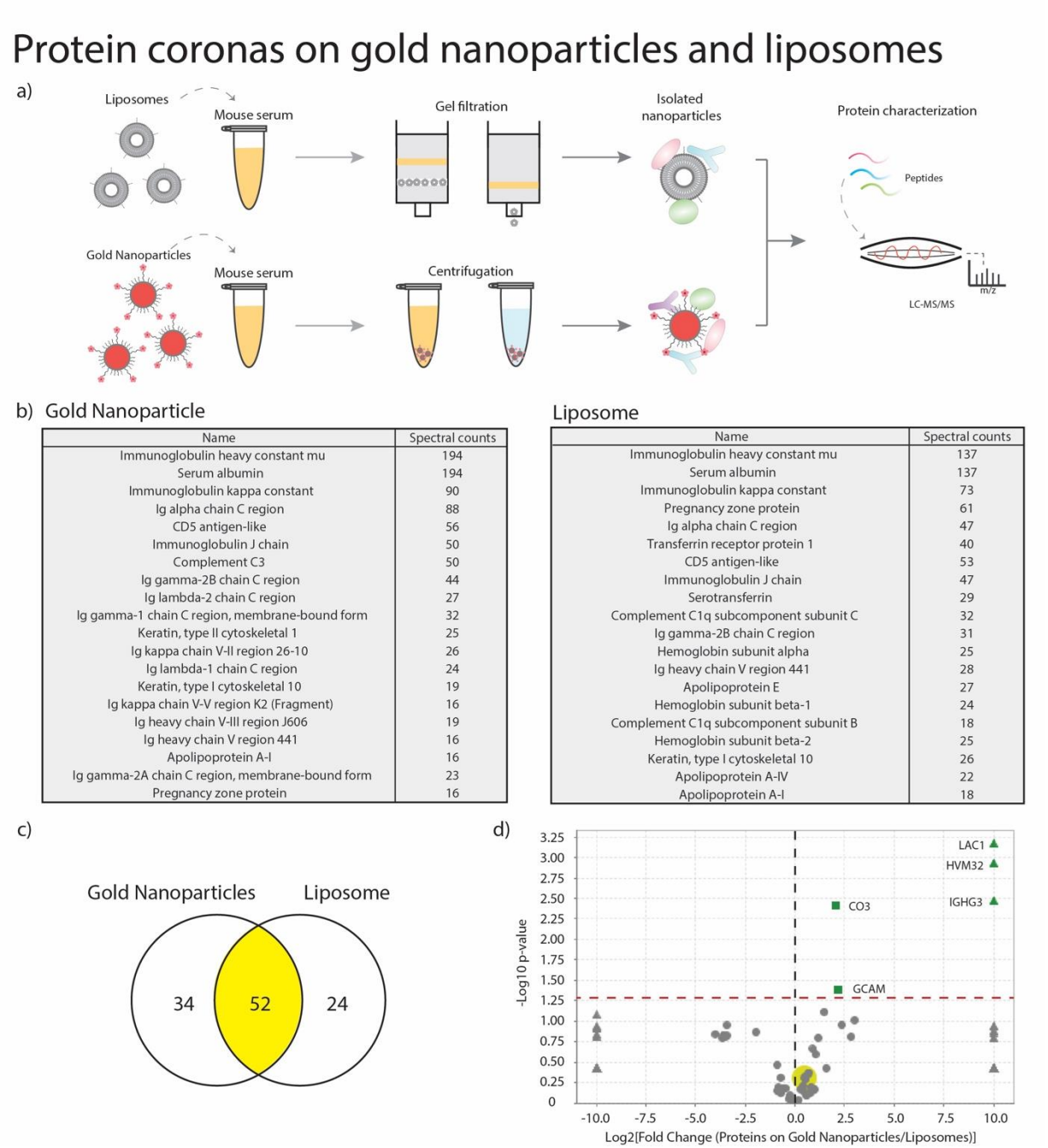


| Name | Spectral counts |
|---|---|
| Immunoglobulin heavy constant mu | 194 |
| Serum albumin | 194 |
| Immunoglobulin kappa constant | 90 |
| Ig alpha chain C region | 88 |
| CD5 antigen-like | 56 |
| Immunoglobulin J chain | 50 |
| Complement C3 | 50 |
| Ig gamma-2B chain C region | 44 |
| Ig lambda-2 chain C region | 27 |
| Ig gamma-1 chain C region, membrane-bound form | 32 |
| Keratin, type II cytoskeletal 1 | 25 |
| Ig kappa chain V-II region 26-10 | 26 |
| Ig lambda-1 chain C region | 24 |
| Keratin, type I cytoskeletal 10 | 19 |
| Ig kappa chain V-V region K2 (Fragment) | 16 |
| Ig heavy chain V-III region J606 | 19 |
| Ig heavy chain V region 441 | 16 |
| Apolipoprotein A-I | 16 |
| Ig gamma-2A chain C region, membrane-bound form | 23 |
| Pregnancy zone protein | 16 |

| Name | Spectral counts |
|---|---|
| Immunoglobulin heavy constant mu | 137 |
| Serum albumin | 137 |
| Immunoglobulin kappa constant | 73 |
| Pregnancy zone protein | 61 |
| Ig alpha chain C region | 47 |
| Transferrin receptor protein 1 | 40 |
| CD5 antigen-like | 53 |
| Immunoglobulin J chain | 47 |
| Serotransferrin | 29 |
| Complement C1q subcomponent subunit C | 32 |
| Ig gamma-2B chain C region | 31 |
| Hemoglobin subunit alpha | 25 |
| Ig heavy chain V region 441 | 28 |
| Apolipoprotein E | 27 |
| Hemoglobin subunit beta-1 | 24 |
| Complement C1q subcomponent subunit B | 18 |
| Hemoglobin subunit beta-2 | 25 |
| Keratin, type I cytoskeletal 10 | 26 |
| Apolipoprotein A-IV | 22 |
| Apolipoprotein A-I | 18 |

**Supplementary Figure 41 | Adsorbed proteins on gold nanoparticles and liposomes** **(a)** Experimental schematic. The liposomes and gold nanoparticles were first incubated with the pooled mouse serum for one hour at 37ºC to allow serum proteins to adsorb. The protein-liposome complexes were separated from unbound proteins by size exclusion chromatography and concentrated with ultra-centrifugation. The protein-gold nanoparticle complexes were separated through centrifugation washing three times. Next, the adsorbed proteins were isolated from the nanoparticle surface and trypsinized into peptides. They were then identified and quantified on LC-MS/MS. **(b)** The top 20 adsorbed proteins identified on gold nanoparticles and liposomes. (n=3, Pearson correlation between replicates AuNPs: 0.93, Liposomes: 0.77). **(c)** Venn diagram of shared and unique proteins on gold nanoparticles and liposomes. **(d)** A volcano

plot of proteins adsorbed on gold nanoparticles and liposomes. Proteins highlighted in green were statistically significantly more abundant on gold nanoparticles. LAC1 is the Ig lambda-1 chain C region. HVM32 is the Ig heavy chain V-III region J606. IGHG3 is the Ig gamma-3 chain C region. CO3 is the Complement C3. GCAM is Ig gamma-2A chain C region, membrane-bound form. (Red line: $p<0.05$). Statistical significance was evaluated using a two-tailed unpaired t-test between protein values of liposome and gold for each protein.

## Supplementary Videos

Please see Supplementary Videos in separate files.

**Supplementary Video 1 | Live intravital imaging of Cy3 gold nanoparticle uptake in Kupffer cells in a mouse administered with a low dose**
The livers of Csf1r-EGFP BALB/c mice were imaged. Kupffer cells (blue) were identified and monitored for a few frames, then 0.2 trillion Cy3-labelled gold nanoparticles (red) were injected and imaged for 30 minutes.

**Supplementary Video 2 | Live intravital imaging of Cy3 gold nanoparticle uptake in Kupffer cells in a mouse administered with a high dose**
The livers of Csf1r-EGFP BALB/c mice were imaged. Kupffer cells (blue) were identified and monitored for a few frames, then 0.2 trillion Cy3-labelled gold nanoparticles (red) and 12 trillion Cy5-labelled gold nanoparticles were injected and imaged for 30 minutes. This video shows only the Cy3 and GFP channels to visualize Cy3 nanoparticle uptake.

**Supplementary Video 3 | Live intravital imaging of Cy5 gold nanoparticle uptake in Kupffer cells in a mouse administered with a high dose**
The livers of Csf1r-EGFP BALB/c mice were imaged. Kupffer cells (blue) were identified and monitored for a few frames, then 0.2 trillion Cy3-labelled gold nanoparticles (red) and 12 trillion Cy5-labelled gold nanoparticles were injected and imaged for 30 minutes. This video shows only the Cy5 and GFP channels to visualize Cy5 nanoparticle uptake.

# Supplementary Tables

## Supplementary Table 1 | Included studies from Wilhelm et al.

Studies from Wilhelm et al[1]. Listed are the recalculated doses and the reported tumour delivery, in % injected dose per gram.

| Citation | Dose | Tumour Delivery (% ID/g) | Inorganic or Organic | Material | Active/ Passive | Size (Small/Big) | Tumor model | Cancer type | Cell line |
|---|---|---|---|---|---|---|---|---|---|
| Pathak 2009 | 4.11E+06 | 0.15 | Organic | Polymeric | Passive | Big | Allograft heterotopic | Breast adenocarcinoma | Ehrlich ascites tumor cell |
| Pathak 2009 (2) | 1.29E+07 | 1.17 | Organic | Polymeric | Passive | Big | Allograft heterotopic | Breast adenocarcinoma | Ehrlich ascites tumor cell |
| Wang 2015 | 9.76E+09 | 0.83 | Inorganic | Other | Passive | Small | Allograft heterotopic | Breast | 4T1 |
| Wu 2013 | 9.85E+09 | 0.38 | Organic | Hydrogel | Passive | Big | Xenograft heterotopic | Brain | U87MG |
| Chakravarty 2015 | 1.80E+10 | 3 | Inorganic | Silica | Passive | Big | Xenograft heterotopic | Brain | U87MG |
| Chakravarty 2015 (2) | 1.80E+10 | 4.5 | Inorganic | Silica | Active | Big | Xenograft heterotopic | Brain | U87MG |
| Behnam Azad 2015 | 3.00E+10 | 4.3 | Inorganic | Iron Oxide | Active | Big | Xenograft heterotopic | Prostate | PSMA |
| Arnida 2011 | 4.70E+10 | 0.3 | Inorganic | Gold | Passive | Big | Xenograft orthotopic | Ovarian cancer | A2780 |
| Chen 2015 | 5.25E+10 | 1.3 | Inorganic | Other | Passive | Big | Xenograft heterotopic | Breast | MCF-7 |
| Chen 2015 (2) | 5.25E+10 | 6 | Inorganic | Other | Active | Big | Xenograft heterotopic | Breast | MCF-7 |
| Chu 2013 (2) | 5.88E+10 | 0.01 | Organic | Polymeric | Passive | Big | Xenograft heterotopic | Lung | A549 |
| Dam 2015 | 7.59E+10 | 2 | Inorganic | Gold | Active | Small | Xenograft heterotopic | Breast | MDA-MB-231 |
| Kennedy 2011 | 1.00E+11 | 0.5 | Inorganic | Gold | Passive | Big | Xenograft heterotopic | Lymphoblastoid | LCL |
| Guo 2013 | 1.51E+11 | 2 | Organic | Polymeric | Passive | Big | Allograft heterotopic | Breast | 4T1 |
| Guo 2013 (2) | 1.51E+11 | 4.3 | Organic | Polymeric | Active | Big | Allograft heterotopic | Breast | 4T1 |
| Dam 2015 (2) | 1.52E+11 | 6 | Inorganic | Gold | Active | Small | Xenograft heterotopic | Breast | MDA-MB-231 |
| Cabral 2011 (4) | 1.83E+11 | 8 | Organic | Polymeric | Passive | Big | Xenograft heterotopic | Pancreas | BxPC3 |
| Cabral 2011 (8) | 1.83E+11 | 4 | Organic | Polymeric | Passive | Big | Xenograft heterotopic | Pancreas | BxPC3 |
| Sykes 2014 (2) | 2.00E+11 | 5 | Inorganic | Gold | Passive | Big | Xenograft orthotopic | Skin | MDA-MB-435 |
| Sykes 2014 (6) | 2.00E+11 | 9 | Inorganic | Gold | Active | Big | Xenograft orthotopic | Skin | MDA-MB-435 |
| Chu 2013 | 3.71E+11 | 0.19 | Organic | Polymeric | Passive | Big | Xenograft heterotopic | Lung | A549 |
| Sykes 2014 (3) | 6.00E+11 | 15 | Inorganic | Gold | Passive | Big | Xenograft orthotopic | Skin | MDA-MB-435 |
| Sykes 2014 (7) | 6.00E+11 | 22 | Inorganic | Gold | Active | Big | Xenograft orthotopic | Skin | MDA-MB-435 |
| Cabral 2011 (3) | 7.17E+11 | 10 | Organic | Polymeric | Passive | Big | Xenograft heterotopic | Colon adenocarinoma | C26 |
| Cabral 2011 (7) | 7.17E+11 | 4 | Organic | Polymeric | Passive | Big | Xenograft heterotopic | Pancreas | BxPC3 |
| Shah 2012 | 8.05E+11 | 3 | Inorganic | Gold | Passive | Big | Xenograft heterotopic | Prostate | LNCaP |
| Arnida 2011 (2) | 8.80E+11 | 1.8 | Inorganic | Gold | Passive | | Xenograft orthotopic | Ovarian cancer | A2780 |

| | | | | | | | | | |
|---|---|---|---|---|---|---|---|---|---|
| Gormley 2011 | 8.90E+11 | 7.80E+00 | Inorganic | Gold | Passive | | Xenograft heterotopic | Pancreas | Panc-1 |
| Gormley 2011 (2) | 8.90E+11 | 1.56E+00 | Inorganic | Gold | Active | | Xenograft heterotopic | Pancreas | Panc-1 |
| Wu 2015 | 9.92E+11 | 9 | Organic | Hydrogel | Passive | Big | Allograft heterotopic | Hepatoma | H22 |
| Chen 2012 | 1.15E+12 | 4 | Inorganic | Silica | Passive | Big | Allograft heterotopic | Breast | 4T1 |
| Chen 2008 | 1.2E+12 | 0.7 | Inorganic | Other | Passive | Small | Allograft heterotopic | Colon adenocarinoma | C26 |
| Chen 2008 (2) | 1.2E+12 | 4 | Inorganic | Other | Active | Small | Allograft heterotopic | Colon adenocarinoma | C26 |
| Cai 2007 | 1.20E+12 | 0.7 | Inorganic | Other | Passive | Small | Xenograft heterotopic | Brain | U87MG |
| Cai 2007 (2) | 1.20E+12 | 4.3 | Inorganic | Other | Active | Small | Xenograft heterotopic | Brain | U87MG |
| Wang 2014 | 1.45E+12 | 2.5 | Organic | Hydrogel | Passive | Big | Allograft heterotopic | Hepatoma | H22 |
| Wang 2014 (2) | 1.45E+12 | 2.5 | Organic | Hydrogel | Active | Big | Allograft heterotopic | Hepatoma | H22 |
| Goodrich 2010 | 1.60E+12 | 1.92 | Inorganic | Gold | Passive | Small | Allograft heterotopic | Colon adenocarinoma | C26 |
| Cabral (6) | 1.68E+12 | 7 | Organic | Polymeric | Passive | Big | Xenograft heterotopic | Colon adenocarinoma | C26 |
| Cabral 2011 (2) | 1.68E+12 | 9 | Organic | Polymeric | Passive | Big | Xenograft heterotopic | Colon adenocarinoma | C26 |
| Sykes 2014 (4) | 2.00E+12 | 18 | Inorganic | Gold | Passive | Big | Xenograft orthotopic | Skin | MDA-MB-435 |
| Sykes 2014 (8) | 2.00E+12 | 27 | Inorganic | Gold | Active | Big | Xenograft orthotopic | Skin | MDA-MB-435 |
| Liu 2014 | 2.40E+12 | 1 | Inorganic | Gold | Passive | Small | Xenograft heterotopic | Cervical | KB |
| Cheng | 2.40E+12 | 2.5 | Inorganic | Gold | Passive | Small | Xenograft heterotopic | Brain | U87MG |
| Cheng (2) | 2.40E+12 | 8 | Inorganic | Gold | Active | Small | Xenograft heterotopic | Brain | U87MG |
| Wong 2013 | 3.00E+12 | 6 | Organic | Liposomes | Passive | Big | Allograft orthotopic | Breast | MET1 |
| Liu 2007 | 3.61E+12 | 3 | Organic | Other | Passive | | Xenograft heterotopic | Brain | U87MG |
| Liu 2007 (2) | 3.61E+12 | 3 | Organic | Other | Passive | | Xenograft heterotopic | Brain | U87MG |
| Liu 2007 (3) | 3.61E+12 | 13 | Organic | Other | Active | | Xenograft heterotopic | Brain | U87MG |
| Hu 2015 | 4E+12 | 6.49 | Organic | Polymeric | Passive | Small | Xenograft heterotopic | Brain | U87MG |
| Negi 2014 | 5.20E+12 | 3 | Organic | Liposomes | Passive | Big | Allograft heterotopic | Breast adenocarcinoma | Ehrlich ascites tumor cell |
| Perez-Medina 2014 | 5.43E+12 | 13.7 | Organic | Liposomes | Passive | Big | Allograft heterotopic | Breast | 4T1 |
| Kirpotin 2006 | 6.76E+12 | 8 | Organic | Liposomes | Passive | Big | Xenograft heterotopic | Breast | BT474 |
| Kirpotin 2006 (2) | 6.76E+12 | 8 | Organic | Liposomes | Active | Big | Xenograft heterotopic | Breast | BT474 |
| Zhong 2015 | 7.12E+12 | 17 | Inorganic | Gold | Passive | Small | Xenograft heterotopic | Cervical | HeLA |
| Chang 2010 | 7.17E+12 | 6.1 | Organic | Liposomes | Passive | Big | Allograft heterotopic | Colon adenocarinoma | C26 |
| Okuda 2006 | 7.17E+12 | 14.5 | Organic | Hydrogel | Passive | Small | Allograft heterotopic | Colon adenocarinoma | C26 |
| Shi 2015 | 9.61E+12 | 8 | Organic | Polymeric | Passive | Big | Xenograft orthotopic | Skin | A431 |
| Sykes 2014 | 1.00E+13 | 20 | Inorganic | Gold | Passive | Small | Xenograft orthotopic | Skin | MDA-MB-435 |
| Sykes 2014 (5) | 1.00E+13 | 30 | Inorganic | Gold | Active | Small | Xenograft orthotopic | Skin | MDA-MB-435 |
| Lee 2011 | 1.20E+13 | 7.91 | Organic | Liposomes | Passive | Big | Xenograft heterotopic | Brain | U87MG |
| Song 2014 | 1.38E+13 | 8 | Organic | Liposomes | Passive | Big | Allograft orthotopic | Breast | T11 gem |

| | | | | | | | | | |
|---|---|---|---|---|---|---|---|---|---|
| Cabral 2011 (1) | 1.39E+13 | 10 | Organic | Polymeric | Passive | Small | Xenograft heterotopic | Colon adenocarinoma | C26 |
| Cabral 2011 (5) | 1.39E+13 | 11 | Organic | Polymeric | Passive | Small | Xenograft heterotopic | Pancreas | BxPC3 |
| Khalid 2006 | 6.16E+13 | 10.5 | Organic | Liposomes | Passive | Big | Allograft heterotopic | Colon adenocarinoma | C26 |
| DeNardo 2007 | 1.04E+14 | 12.5 | Inorganic | Iron Oxide | Active | Small | Xenograft heterotopic | Breast | HBT3477 |
| Zolata 2014 | 3E+16 | 10 | Inorganic | Gold/iron | Active | Small | Xenograft heterotopic | Breast | SKBR3 |

1
2

**Supplementary Table 2 | Excluded studies from Wilhelm et al.**

Studies from Wilhelm et al[1]. We were unable to calculate doses of these studies and so we excluded them from the analysis. The reasons for exclusion are given.

| Study (Author, year) | Reasons for exclusion |
|---|---|
| Zhang 2015 | Ultrasmall; exclude |
| Meyers 2015 | Pc4 dose given; gold dose unclear |
| Hu 2014 | Dosing given in radioactivity, not particles |
| Razzak 2013 | Can't find reference |
| Zhang 2015 | Ultrasmall; exclude |
| Black 2014 | Only reported radioactive dose; unclear how gold dose determined |
| Liu 2013 | Ultrasmall; exclude |
| Karmani 2013 | Only reported radioactive dose; unclear how gold dose determined |
| Wang 2012 | Only reported radioactive dose; unclear how gold dose determined |
| Perrault 2009 | Can't figure out the delivery from the log graphs |
| Yang 2013 | Dose unclear; it's a mixed element nanoparticle |
| Chauhan 2013 | Excluded b/c values don't make sense (see blood in figure 9a) |
| Chauhan 2013 | Unclear conjugation/radiolabelling amounts |
| Yang 2011 | Unclear conjugation/labelling amounts |
| Quan 2011 | Signal appears to be noise |
| Goel 2014 | Unclear conjugation/radiolabelling amounts |
| Chen 2014 | Unclear conjugation/radiolabelling amounts |
| Chen 2014 | Unclear conjugation/radiolabelling amounts |
| Benezra 2011 | Total accumulation in all organs is <10% at 24h; excluded. |
| Chen 2013 | Unclear conjugation/radiolabelling amounts |
| Hu 2013 | Total accumulation in all organs is <10% at 24h; excluded. |
| Yu 2015 | Unconventional shape and hard to calculate dose |
| Zhang 2013 | ip injection; exclude |
| Mi 2014 | Unclear how many Gd per CaP nanoparticle; exclude |
| Huang 2015 | Dose unclear |
| Hong 2015 | 0.97 GBq/mg; unclear what the size is; exclude |
| Al-Jamal 2009 | Unclear how many QD per liposome |
| Kai 2015 | Only relative AUC is given and not sure what the %ID is; exclude |
| Chen 2015 | Recovery <10%; exclude |
| Oliveira 2014 | Bunch of AUCs and unclear what %ID/g is; exclude |
| Polyak 2013 | Rat; unclear conjugation/radiolabelling amounts; exclude |
| Ding 2013 | Recovery <10%; exclude |
| Chu 2013 | Only AUC given; Unclear the %ID/g; exclude |
| Ma 2012 | Recovery <10%; exclude |

| | |
|---|---|
| Guo 2013 | 4.6 wt% dox; recovery <10%; exclude |
| Sumitani 2011 | Unclear dose; exclude |
| Bae 2007 | Unclear dose (mmol wt %???); exclude |
| Cabral 2004 | Dose unclear |
| Bibby 2005 | Dox is 3.3 wt %; thus 7.6 mg of polymer injected per mouse; Size/density unclear - exclude |
| Bae 2005 | Loading effciency and density unclear; exclude |
| van Vlerken 2008 | Recovery <10% and <24h study; exclude |
| Sasatsu 2008 | Density unclear; exclude |
| Rossin 2005 | Density/radiolabelling unclear; exclude |
| Mondal 2010 | 94% radiolabelling effociency; dose of particle unclear |
| He 2010 | Density unclear; exclude |
| Cabral 2007 | Loading efficiency and density unclear; exclude |
| Shi 2013 | Unclear conjugation/radiolabelling amounts |
| Hong 2012 | Unclear conjugation/radiolabelling amounts |
| Xu 2015 | Recovery <10%+unclear size dimensions; exclude |
| Shi 2014 | Unclear conjugation/radiolabelling amounts |
| Hong 2012 | Unclear conjugation/radiolabelling amounts |
| Lin 2014 | Unclear conjugation/radiolabelling amounts |
| Hirsjarvi 2013 | Unclear what ingredients they're using to calculate dose |
| Lin 2011 | Unclear how to convert phospholipids to liposomes |
| Miyajima 2006 | Unclear what concentration was |
| Paolino 2010 | DPPC:Chol:PEG at 6:3:1; recovery <10% = exclude |
| Zamboni 2007 | Unclear loading amount - exclude |
| Chen 2008 | IP administration; exclude |
| Yuan 2006 | Recovery <10%; exclude |
| Chen 2010 | Unclear radiolabelling amount; exclude |
| Chang 2007 | Unclear radiolabelling amount; exclude |
| Han 2015 | Unclear liposome ingredients and loading ratios |
| Yang 2015 | 16% wt loading; Recovery <10% exclude |
| Ganesh 2013 | Recovery <10% exclude |
| Xu 2013 | Unclear accumulation at 24h (log scales); exclude |
| Cheng 2012 | Recovery <10% exclude |
| Kommareddy 2007 | Unclear radiolabelling |
| Qian 2014 | Recovery <10% exclude |
| Sadekar 2011 | Recovery <10% exclude |
| Kukowska-Latallo 2005 | Recovery <10% exclude |
| Zhang 2015 | Rats; exclude |
| Chen 2015 | Unclear gold:particle ratio; exclude |
| Balogh 2007 | Unclear dose; exclude |
| Sadekar 2012 | Unclear dose; exclude |
| Tian 2015 | Unclear size/doses; exclude |

| | |
|---|---|
| Kim 2015 | Recovery <10%; exclude |
| Harivardhan 2005 | Recovery <10%; exclude |
| Lee 2013 | Unclear density of upconverting particle; excluded |

1
2

**Supplementary Table 3 | Multiple regression analysis of Wilhelm et al.**

Output tables from SPSS multiple regression analysis of Wilhelm et al.[1]

### 3a. Model Summary

| Model | R | R Square | Adjusted R Square | Std. Error of the Estimate | Change Statistics | | | | |
|---|---|---|---|---|---|---|---|---|---|
| | | | | | R Square Change | F Change | df1 | df2 | Sig. F Change |
| 1 | 0.711 | 0.506 | 0.434 | 4.83227 | 0.506 | 7.036 | 8 | 55 | 0.000 |

### 3b. Coefficients of the model.

The model is of the general form

$$delivery = \beta_i x_i + constant$$

where $x_i$ are the variables listed below and $\beta_i$ are their corresponding coefficients:

| Variable | Unstandardized Coefficients | | Standardized Coefficients | t | Sig. | 95.0% Confidence Interval for B | |
|---|---|---|---|---|---|---|---|
| | B | Std. Error | Beta | | | Lower Bound | Upper Bound |
| (Constant) | -37.554 | 9.337 | | -4.022 | 0.00000 | -56.265 | -18.843 |
| Dose (log) | 3.395 | 0.734 | 0.48 | 4.622 | 0.00002 | 1.923 | 4.867 |
| Cancer Type | 0.565 | 0.199 | 0.368 | 2.844 | 0.00600 | 0.167 | 0.963 |
| Active vs Passive | -3.918 | 1.454 | -0.276 | -2.696 | 0.00900 | -6.831 | -1.005 |
| Size | 1.504 | 1.073 | 0.142 | 1.402 | 0.16700 | -0.646 | 3.653 |
| Tumor Model | 0.896 | 0.832 | 0.143 | 1.077 | 0.28600 | -0.771 | 2.564 |
| Cell Line | 0.083 | 0.107 | 0.098 | 0.779 | 0.44000 | -0.131 | 0.298 |
| Inorganic vs Organic | 0.705 | 1.735 | 0.055 | 0.406 | 0.68600 | -2.773 | 4.183 |
| Material | -0.098 | 0.316 | -0.039 | -0.311 | 0.75700 | -0.733 | 0.536 |

**Supplementary Methods**

Modelling.

Kinetic accumulation in the liver and tumour were modelled using a compartment model composed of 4 compartments: blood, liver (Kupffer cell), liver (other cells), and other organs. The following assumptions were made: the blood compartment started at 100% and delivered nanoparticles to all other compartments, nanoparticles were always perfectly mixed in the blood (i.e. no local concentration differences), flow of nanoparticles from other compartments back into blood was negligible, flow of nanoparticles between non-blood compartments is negligible, and all compartments had a finite capacity. The compartment model, outlined in Figure 12a, dictates the following equations:

$$NP + T \leftrightharpoons_{k-T}^{kT} NPT \quad (1)$$

$$NP + KCM - KC \leftrightharpoons_{k-KC}^{kKC} NPKCM \quad (2)$$

$$NPKCM + KC \leftrightharpoons_{k-OC}^{kOC} NPKC \quad (3)$$

$$NP + O \leftrightharpoons_{k-O}^{kO} NPO \quad (4)$$

where NP is the concentration of total circulating nanoparticles and T, KCM, KC, and O are the concentrations of remaining capacity in each of the compartments: Tumour, Kupffer Cell Membranes, Kupffer Cells, Other organs. NPT, NPKCM, NPKC, and NPO are the concentrations of nanoparticles in each of these compartments. Each $k_x$ represents the rate of the transfer of nanoparticles from blood to the respective compartment, and $k_{-x}$ represents transfer of nanoparticles from organ back to blood (negligible). These rate equations can described by a system of ordinary differential equations:

$$\frac{dNP}{dt} = -k_T NP(T_0 - NPT) - k_{L,bind} NP(KCM_0 - NPKCM) - k_O NP(O_0 - NPO) \quad (5)$$

$$\frac{dNPT}{dt} = k_T NP(T_0 - NPT) \quad (6)$$

$$\frac{dNPKCM}{dt} = k_{L,bind} NP(KCM_0 - NPKCM) - k_{L,uptake} KC(KC_0 - NPKC) \quad (7)$$

$$\frac{dNPKC}{dt} = k_{L,uptake} KC(KC_0 - NPKC) \quad (8)$$

$$\frac{dNPO}{dt} = k_O NP(O_0 - NPO) \quad (9)$$

where $T_0$, $KCM_0$, $KC_0$, $O_0$ are boundary conditions for organ weight-normalized capacities of the tumour, Kupffer cell membranes, Kupffer cell endosomes, and other organ compartments. We limited $KCM_0$ to be 1 trillion nanoparticles/gram. We set *k* values such that $k_{KCM} > k_O > k_{KC} > k_T$. We used two doses, 50 trillion and 0.2 trillion. Using these equations and initial conditions, we simulated the evolution of nanoparticle concentrations in these compartments over 24 hours using MATLAB's ode23 function. To decrease computational time, we decreased the doses by 1e10 and the *k* constants accordingly. All code is available on the github repository online at the URL: https://github.com/beeno/trillionParticlesODEs

Transmission electron microscopy.

Samples for TEM were fixed in 2% (v/v) paraformaldehyde and 2.5% (v/v) glutaraldehyde in 0.1 M sodium cacodylate buffer, rinsed in buffer, post-fixed in 1% osmium tetroxide in buffer, dehydrated in a graded ethanol series followed by propylene oxide, and embedded in Quetol-Spurr resin. Sections 90nm thick were cut on a Leica EM UC7 ultramicrotome, stained with uranyl acetate and lead citrate and viewed in an FEI Tecnai 20 TEM. Sample preparation and imaging was done at the Nanoscale Biomedical Imaging Facility (SickKids, Toronto, Canada).

Caelyx biodistribution.

Doxorubicin was extracted from mouse tissues as previously described[2]. Briefly, mice were anesthetized with 3% (v/v) isoflurane with 0.5 L/minute of oxygen. The thoracic cavity was dissected and heart exposed. Intracardiac blood was collected using a 25G needle and syringe and expelled without needle into a 1.5 mL centrifuge tube. This was allowed to clot at room temperature for 30 minutes, then centrifuged at 2000 x g for 10 minutes. Plasma was collected and stored at -20ºC. The liver and tumour were dissected, weighed, frozen, lyophilized, and weighed again. Water was added to a concentration of 10% w/v dry weight. Tissues were homogenized using a gentleMACS Octo Dissociator (Miltenyi Biosystems) in gentleMACS M Tubes (Miltenyi Biosystems) on the "RNA frozen" setting. 0.150 mL of homogenates were transferred to a 1.5 mL centrifuge tube containing an extraction buffer of 1.125 mL acidified isopropanol (0.75 N), 0.14 mL $H_2O$, 0.075 mL Triton X-100. 0.150 mL of the injection dose was diluted in a standard curve from 0.002% to 83% and added to the same extraction buffer. Doxorubicin was extracted overnight at -30ºC. The following day, samples were warmed to room temperature, vortexed for 30 seconds, and then centrifuged at 15,000 x g for 20 minutes. The supernatant was collected and pellet discarded. 150 µL of supernatant was added to a black 96 well plate (Greiner 655086) and read on a fluorescence plate reader (Tecan Infinite 200 PRO) at excitation/emission 470 nm/585 nm. Percent injected dose was compared to values of the standard curve.

Caelyx tumour uptake analysis.

Mice with 1-week old tumours were sacrificed 1-4 days after the injection of Caelyx or Caelyx + delivery enhancers. Tumours were cryopreserved in "optimum cutting temperature" compound

(VWR 25608-930) and indirect contact with liquid nitrogen. Histological slides were processed at the The Centre for Phenogenomics. Briefly, 8µm thick sections were sectioned on a Cryostar NX70 cryostat, stained with anti-CD31 (Abcam ab28364), and imaged using an Olympus VS120 microscope. Doxorubicin-positive nuclei and all nuclei were thresholded and counted in ImageJ. The ratio between them was used to calculate the percent-positive doxorubicin nuclei in slides.

Delivery enhancer toxicity analysis

2 days and 2 weeks after injection, ~100 µL of mouse whole blood was collected from the tail vein into heparinized collection tubes. Samples were kept on ice and transferred to the Division of Comparative Medicine (University of Toronto) for complete blood cell counts (VetScan HM5; Abaxis Inc.). 2 weeks and 1.4 years after injection, ~400 µL of whole blood was collected via cardiac puncture and allowed to coagulate in 1.5 mL tubes for 30-60 minutes at room temperature, then centrifuged at 2000xg for 10 minutes. Serum was removed and stored at -80ºC until analysis. Serum was analyzed at The Centre for Phenogenomics (Toronto, ON) for liver and lipid biomarkers. In addition to blood, the liver and heart were also excised and preserved in neutral buffered formalin for 24 hours, then preserved in 70% ethanol. These tissues were processed into paraffin blocks, cut, and stained by the Toronto Centre for Phenogenomics for H&E. Sections were scanned at 20x-40x.

Liver perfusion and disaggregation for single cell analysis.

The mouse was anesthetized using isoflurane (5% induction, 2% maintenance). A horizontal skin incision was made across the abdomen midline. Skin was retracted and the same incision was made onto the peritoneum to expose the viscera. Intestines were gently displaced outside to the

left of the mouse to expose the portal vein and vena cava. A 21G needle connected to a peristaltic pump was inserted into the portal vein, the vena cava was cut open (to allow outflow), and perfusion was performed for 5 minutes at 5 mL/minute with a 10 U/mL heparin solution in 1x PBS (calcium-free). The liver was observed to turn in colour from red to brown. The solution was then exchanged for 3 mg/mL collagenase in HBSS at a flow rate of 5 mL/minute for 5 minutes to digest. The liver was observed to turn in colour from brown to tan/yellow. When the colour change was patchy, it indicated suboptimal perfusion; in these cases the 21G was poked into the liver and flow rate was reduced. At the end of digestion, the liver was carefully excised and placed into a solution of HBSS. The Glisson's capsule was cut and the liver was gently agitated with tweezers to dissociate hepatic cells into the solution. This cell solution was centrifuged at 25g for 2 minutes. The supernatant was labelled as non-parenchymal cells and the pellet was labelled as parenchymal cells. A portion of parenchymal cells were visualized under DIC microscopy to assess presence of hepatocytes; if no hepatocytes, we deemed the perfusion/digestion a failure and discarded the sample. Samples were diluted to 25 million cells / mL according to a standardized counter (Beckman Coulter ViCell XR using "default" cell type) and kept on ice. Flow cytometry was performed as described in the main text.

Characterization of adsorbed proteins on gold nanoparticles and liposomes

All nanoparticle numbers were increased compared to *in* vivo doses to be able to extract enough protein for analysis. 1.2 trillion PEGylated gold nanoparticles in 100 μL PBS were added to 1 mL of pooled mouse serum (Sigma Aldrich M5905) and incubated at 37ºC for one hour. To isolate these protein-coated nanoparticles, the solution was centrifuged at 1,600 g for 30 minutes to pellet. Gold nanoparticles were resuspended in 950 μL PBS with 0.02% Tween20. This

washing process was repeated three more times. The protein corona on liposomes was prepared similarly. 115 trillion liposomes in 100 µL PBS (80 mg of lipid/mL) were added to 1 mL of mouse serum and incubated for one hour at 37ºC. The isolation of protein-coated liposomes from unbound proteins was different from gold nanoparticles because liposomes require high centrifugal forces to pellet that would pull down large proteins that are unbound. So first, size exclusion chromatography adopted from previous studies was used[3–5]. Briefly, 500 µL of the serum and liposome mixture was applied to a column (13 cm x 1.5 cm) packed with Sepharose CL-4B (GE life sciences 17-0150-01). The column was eluted with PBS and the fraction with liposomes were collected. To further concentrate the sample, 2 mL of the sample was layered on top of a cushion of 100 µL of 1 M sucrose (BioShop) at the bottom of the centrifugation tube, and then centrifuged at 50,000 g for 30 minutes. (Optima™ MAX-XP; Rotor: TLA110; Tube: Ultra-Clear™ 13 x 51 mm).

Protein coated gold nanoparticles and liposomes (40 µL) were transferred to a new tube for further purification. 20 µL of sodium dodecyl sulfate (SDS) and 20 µL of 200 mM dithiothreitol (DTT) were then added and incubated at 80°C for 10 minutes. The samples were then centrifuged at 18,000 g for 15 minutes, and 60 µL of the supernatant with extracted proteins were transferred to a new tube. The extracted proteins were then purified through acetone precipitation as described[6]. Briefly, 950 µL of trichloroacetic acid (TCA) (10% w/v in acetone) was added to each sample and incubated at -80 °C overnight. The samples were then centrifuged at 18,000 g at room temperature for 15 minutes, and the supernatant was discarded. 500 µL of sodium deoxycholic acid (SDC) was added to the pellet and vortexed thoroughly. Next, 100 µL of trichloroacetic acid (72% w/v in water) was added, and samples were left on ice for 2 hours. The

samples were then centrifuged at 15,000 g for 15 minutes. The supernatant was discarded, and 950 µL of acetone was added. The samples were left at -80 °C overnight and centrifuged at 18,000 g for 15 minutes. The supernatant was discarded, and the samples were left to air dry. Isolated and purified protein corona on AuNPs and liposomes were then processed for characterization by liquid chromatography-tandem mass spectrometry (LC-MS/MS). 45 µL of 100 mM ammonium bicarbonate ($NH_4HCO_3$) and 5 µL of acetonitrile (ACN) was first added to samples. Additional 5 µL of 100 mM DTT was added. The samples were incubated at 37 °C for 60 minutes. 5 µL of an alkylating agent iodoacetamide (500 mM) in 100 mM $NH_4HCO_3$ was added. The solution was kept in the dark for one hour. This was followed by 2 µL of 0.25 µg/µL trypsin solution to digest the peptides. The digestion was stopped by adding 5 µL of 20% v/v formic acid. The proteomic analysis of these processed peptides is carried under the same steps and instrumentation settings as described previously[7]. Briefly, peptides were desalted on a C18 LC column before applying to the column. The elution takes place over one hour at a flow rate of 250 nL/min under 0 to 35 % ACN gradient. Peptides were analyzed on a linear ion trap-Orbitrap hybrid analyzer, LTQ-Orbitrap Elite hybrid mass spectrometer (ThermoFisher). Spectral counts of each protein were then analyzed in Scaffold (Proteome Software).

Data availability.

The authors declare that the data supporting the findings of this study are available within the paper and its supplementary information files. The raw data supporting the findings of this study are available from the corresponding author upon reasonable request. Additional data from the meta-analysis of literature is available from the Cancer Nanomedicine Repository: http://inbs.med.utoronto.ca/cnr/.

Code availability.

All code (used to run the simulation data in Supplementary Figures 12,13) is available on the github repository online at the URL: https://github.com/beeno/trillionParticlesODEs. All code for 3D image analysis can be found on GitHub at the link: https://github.com/BenKingston/nanoparticle_vessel_analysis.

## Supplementary References


1. Wilhelm, S. *et al.* Analysis of nanoparticle delivery to tumours. *Nat. Rev. Mater.* **1**, 1–12 (2016).
2. Charrois, G. J. R. & Allen, T. M. Multiple injections of pegylated liposomal doxorubicin: Pharmacokinetics and therapeutic activity. *J. Pharmacol. Exp. Ther.* **306**, 1058–1067 (2003).
3. Hadjidemetriou, M. *et al.* The Human In Vivo Biomolecule Corona onto PEGylated Liposomes: A Proof-of-Concept Clinical Study. *Adv. Mater.* **31**, 1–9 (2019).
4. Hadjidemetriou, M., Al-Ahmady, Z. & Kostarelos, K. Time-evolution of in vivo protein corona onto blood-circulating PEGylated liposomal doxorubicin (DOXIL) nanoparticles. *Nanoscale* **8**, 6948–6957 (2016).
5. Kristensen, K., Engel, T. B., Stensballe, A., Simonsen, J. B. & Andresen, T. L. The hard protein corona of stealth liposomes is sparse. *J. Control. Release* **307**, 1–15 (2019).
6. Walkey, C. D. *et al.* Protein Corona Fingerprinting Predicts the Cellular Interaction of Gold and Silver Nanoparticles. *ACS Nano* **8**, 2439–2455 (2014).
7. Lazarovits, J. *et al.* Supervised Learning and Mass Spectrometry Predicts the in Vivo Fate of Nanomaterials. *ACS Nano* **13**, 8023–8034 (2019).